
The least-control principle for learning at equilibrium

Alexander Meulemans*
Institute of Neuroinformatics
University of Zürich & ETH Zürich
ameulema@ethz.ch

Nicolas Zucchet*
Department of Computer Science
ETH Zürich
nzucchet@inf.ethz.ch

Seijin Kobayashi*
Institute of Neuroinformatics
University of Zürich & ETH Zürich
seijink@ethz.ch

Johannes von Oswald
Department of Computer Science
ETH Zürich
voswaldj@ethz.ch

João Sacramento
Institute of Neuroinformatics
University of Zürich & ETH Zürich
rjoao@ethz.ch

Abstract

Equilibrium systems are a powerful way to express neural computations. As special cases, they include models of great current interest in both neuroscience and machine learning, such as equilibrium recurrent neural networks, deep equilibrium models, or meta-learning. Here, we present a new principle for learning such systems with a temporally- and spatially-local rule. Our principle casts learning as a *least-control* problem, where we first introduce an optimal controller to lead the system towards a solution state, and then define learning as reducing the amount of control needed to reach such a state. We show that incorporating learning signals within a dynamics as an optimal control enables transmitting credit assignment information in previously unknown ways, avoids storing intermediate states in memory, and does not rely on infinitesimal learning signals. In practice, our principle leads to strong performance matching that of leading gradient-based learning methods when applied to an array of problems involving recurrent neural networks and meta-learning. Our results shed light on how the brain might learn and offer new ways of approaching a broad class of machine learning problems.

1 Introduction

The neural networks of the cortex are both layered and highly recurrent [1, 2]. Their high degree of recurrence and relatively low depth stands in contrast to the prevailing design of artificial neural networks, which have high depth and little to no recurrence. This discrepancy has triggered a recent wave of research into recurrent networks that are more brain-like and which achieve high performance in perceptual tasks [3–7]. Concurrently, another line of recent work has shown that repeating a short sequence of neural computations until convergence can lead to large gains in efficiency, reaching the state-of-the-art in various machine learning problems while reducing model size [8–10].

As we develop models that come closer to cortical networks by way of their recurrence, the precise mechanisms supporting learning in the brain remain largely unknown. While gradient-based methods currently dominate machine learning, standard methods for efficient gradient computation result in non-local rules that are hard to interpret in biological terms [11, 12]. This issue is particularly

*Equal contribution.

aggravated when applying these methods to complex systems involving recurrence [13]. Indeed, while multiple interesting proposals [14–23] have emerged for how to efficiently compute loss function gradients for feedforward networks in biologically-plausible ways, apart from a few notable exceptions [24, 25] much less progress has been made for recurrent networks. In this paper, we focus on the problem of learning such recurrent systems using biologically-plausible local rules. To make progress in this longstanding question we make the assumption that our recurrent system is at equilibrium, and formalize learning as the following optimization problem:

$$\min_{\theta} L(\phi^*) \quad \text{s.t.} \quad f(\phi^*, \theta) = 0, \quad (1)$$

where θ are the parameters we wish to learn, L is a loss function which measures performance, and $\dot{\phi} = f(\phi, \theta)$ is the system dynamics which is at an equilibrium point ϕ^* . Our model is thus *implicitly* defined through a dynamics that is at equilibrium. Expressing our problem in this general form allows us to model a very broad class of learning systems, without being restricted to a particular type of neural network [26–28]. More generally, f is not even restricted to being a neural dynamics. Consider the case where f defines a learning algorithm governing the dynamics of the *weights* of a network; in this case (1) becomes a meta-learning problem, where the goal is to tune the (meta-)parameters of a learning algorithm such that its performance improves.

Inspired by a recent control-based learning method for feedforward neural networks [29], we present a new principle for solving problems of the form (1) which yields learning rules that are (i) gradient-following, (ii) local in space, (iii) local in time, and in particular do not require storing intermediate states, and (iv) not reliant on infinitesimally small learning signals. To meet all four criteria at once, we depart from direct gradient-based optimization of the loss, and we reformulate learning within the framework of optimal control as a *least-control problem*. For this, we use an optimal controller to lead the dynamical system to a minimal-loss equilibrium, and then define learning as reducing the amount of control needed to reach such an equilibrium. Critically, our least-control problem is intimately related to the original learning problem; we make the connection between the two precise by identifying mathematical conditions under which least-control solutions correspond to minima of the original objective $L(\phi^*)$, or a bound of it.

We apply our principle to learn equilibrium recurrent neural networks with a variety of architectures, from laterally-connected networks of leaky integrator neurons to deep equilibrium models [8–10], a recent family of high-performance models which repeat until convergence a sequence of more complex computations. To further demonstrate the generality of our principle, we then consider a recently studied meta-learning problem where the goal is to change the internal state of a complex synapse such that future learning performance is improved [30]. We find that our single-phase local learning rules yield highly competitive performance in both application domains. Our results extend the limits of what can be achieved with local learning rules, opening novel avenues to an old problem.

2 The least-control principle

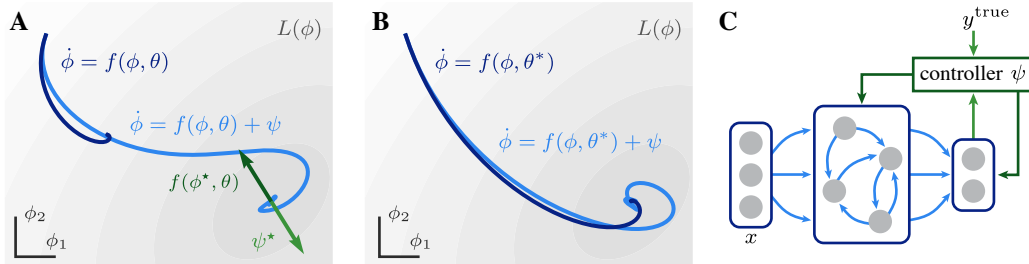


Figure 1: (A, B) Intuition behind the least-control principle. (A) During learning, the free dynamics (dark blue) is augmented with a controller (light blue) that drives the system towards an equilibrium that minimizes the loss function L (grey, the darker the smaller the loss is). Our principle prescribes minimizing the amount of optimal control ψ^* (light green) needed at the equilibrium that minimizes L . (B) After learning, the free equilibrium coincides with the controlled equilibrium and hence minimizes the loss L . (C) Example of an instantiation of the principle on a neural network with recurrent lateral connections within the hidden layer.

2.1 The principle

We introduce the least-control principle for learning dynamical systems $\dot{\phi} = f(\phi, \theta)$ that reach an equilibrium ϕ^* . Instead of directly minimizing a loss evaluated at the equilibrium $L(\phi^*)$ as in (1), we augment the dynamics $\dot{\phi} = f(\phi, \theta) + \psi$ with a control signal ψ that drives the system towards a new controlled equilibrium where the loss is minimized (c.f. Figure 1). Our principle recasts learning as minimizing the amount of control needed to reach that state:

$$\min_{\theta, \phi, \psi} \frac{1}{2} \|\psi\|^2 \quad \text{s.t.} \quad f(\phi, \theta) + \psi = 0, \quad \nabla_{\phi} L(\phi) = 0. \quad (2)$$

The two constraints in the equation above ensure that we reach a steady state of the controlled dynamics, and that the loss L is minimized at this state. Without loss of generality, we consider a single data point above, noting that multiple data points can be handled by considering ϕ and ψ as the concatenated states and controls for all points (c.f. Section S5 in the supplementary materials).

To solve (2), we first fix the parameters θ . We then find an optimal control ψ^* and controlled equilibrium ϕ^* that minimize the following *least-control objective*, for the current setting of θ ,

$$\min_{\phi, \psi} \frac{1}{2} \|\psi\|^2 \quad \text{s.t.} \quad f(\phi, \theta) + \psi = 0, \quad \nabla_{\phi} L(\phi) = 0. \quad (3)$$

Here, ψ^* represents an optimal control with terminal cost $\|\psi\|^2$, and a terminal constraint enforcing that the controlled equilibrium ϕ^* minimizes the loss L . Critically, both credit assignment and system dynamics are now combined into a single phase through the optimal control ψ^* . We then take a gradient-following update in θ on this least-control objective (3), with shorthand notation $\mathcal{H}(\theta) := \frac{1}{2} \|\psi^*\|^2$, which implicitly depends on θ through ψ^* .

Theorem 1 shows that the optimal control signal ψ^* contains enough information about the learning objective so that the gradient is easy to compute. We prove Theorem 1, along with all the theoretical results from Section 2, in Section S2. We use ∂_x to denote partial derivatives w.r.t. the variable x .

Theorem 1 (Informal). *Under some mild regularity conditions, the least-control principle yields the following gradient for θ :*

$$\nabla_{\theta} \mathcal{H}(\theta) = -\partial_{\theta} f(\phi^*, \theta)^{\top} \psi^* = \partial_{\theta} f(\phi^*, \theta)^{\top} f(\phi^*, \theta). \quad (4)$$

The simplicity of our parameter update becomes apparent when contrasting it with the gradient associated with the original objective (1), as the implicit function theorem (c.f. Section S3) gives

$$\nabla_{\theta} L(\phi^*) = -\partial_{\theta} f(\phi^*, \theta)^{\top} (\partial_{\phi} f(\phi^*, \theta))^{-\top} \partial_{\phi} L(\phi^*)^{\top}. \quad (5)$$

Calculating this gradient directly requires inverting the Jacobian $\partial_{\phi} f(\phi^*, \theta)$, which is intractable for large-scale systems. The standard way of dealing with this issue is to resort to the two-phase recurrent backpropagation algorithm [31, 32], which estimates $\nabla_{\theta} L(\phi^*)$ by running a second linear dynamics until equilibrium, while holding the first equilibrium state ϕ^* in memory. This procedure is still more complicated than ours: it requires implementing a specialized auxiliary dynamical system, holding intermediate states in memory, and alternating between inference and gradient computation phases.

To further illustrate what our principle achieves, let us briefly consider the simple setting where $f(\phi, \theta)$ implements a feedforward neural network, typically learned by error backpropagation [33, 34]. In this case, the variable ϕ corresponds to the state of the neurons (representing e.g. their firing rate or postsynaptic voltage) and θ to the synaptic connection weights. The optimal control ψ then drives the network to an equilibrium that minimizes the output loss, while being of minimum norm. The resulting weight update now represents a local Hebbian rule multiplying presynaptic input with the postsynaptic control signal. By contrast, in the backpropagation algorithm errors do not directly influence the neural activity and are computed in a separate phase. In our case, the neural activity implicitly encodes credit assignment information, in such a way that local learning becomes possible.

2.2 A general class of dynamics leads to the same optimal control and parameter update

Our principle is agnostic to the dynamics of the controller $\dot{\psi}(t)$; the only assumption made is that its value ψ_* at the steady state is optimal, i.e. $\psi_* = \psi^*$. We use the subscript $*$ to denote equilibrium

states of the controlled dynamics, the superscript $*$ for a free (not controlled) equilibrium and $*$ to indicate optimality on the least-control objective of Eq. 3. In particular, the parameter update only depends on information available at the controlled equilibrium state (ϕ_*, ψ_*) . Here, we capitalize on this important flexibility by designing different simple feedback controller dynamics that lead to the same optimal steady state. We consider feedback controllers which take the following general form:

$$\dot{\phi} = f(\phi, \theta) + Q(\phi, \theta)u, \quad \text{and} \quad \dot{u} = -\nabla_y L(h(\phi)) - \alpha u, \quad (6)$$

where $y = h(\phi)$ defines a mapping from the system state to an output y on which the loss L is defined, and $Q(\phi, \theta)$ determines the influence of the controller on the system. Here, u may be seen as a leaky integral controller with leak rate α , that uses the output error $\nabla_y L$ to drive the network towards a minimal-loss state (c.f. Section S2). Returning to our example of a neural network, u leads the network into a state configuration where the output neurons y are at a target value.

Theorem 2 provides general conditions for the dynamics (6) to converge to an optimal control signal needed for obtaining first-order parameter updates in Theorem 1.

Theorem 2. *Let (ϕ_*, u_*) be a steady state of the generalized dynamics (6). Assume that $\partial_\phi f(\phi_*, \theta)$ is invertible and that the following column space condition is satisfied at equilibrium:*

$$\text{col}[Q(\phi_*, \theta)] = \text{row}[\partial_\phi h(\phi_*) \partial_\phi f(\phi_*, \theta)^{-1}] \quad (7)$$

Then, $\psi_ = Q(\phi_*, \theta)u_*$ is an optimal control ψ^* for the least-control objective (3), in the limit $\alpha \rightarrow 0$.*

We use leaky integral control in (6) for explanatory purposes and as we use it in our experiments. We remark however that our theory goes beyond this form of output control; in particular, it generalizes to any controller satisfying $\alpha u_* + \nabla_y L(h(\phi_*)) = 0$ at equilibrium. For example, the proportional control $u = -\beta \nabla_y L(\phi)$ with $\beta \rightarrow \infty$ satisfies the condition of Theorem 2, as it has the same steady states as the leaky integral controller of Eq. 6 with $\alpha = \beta^{-1}$.

Interestingly, Theorem 2 shows that many different feedback mappings from the output controller u towards the system state ϕ are possible, as long as the mapping $Q(\phi_*, \theta)$ satisfies the column space condition (7) at equilibrium, in the limit $\alpha \rightarrow 0$. Furthermore, the control ψ need not be instantaneous and can have its own temporal dynamics $\dot{\psi}$ alongside the output controller dynamics \dot{u} , as the column space condition (7) is only defined at equilibrium. We exploit this property and construct a general-purpose algorithm that computes an optimal control ψ^* :

$$\dot{\phi} = f(\phi, \theta) + \psi, \quad \text{and} \quad \dot{\psi} = \partial_\phi f(\phi, \theta)^\top \psi + \partial_\phi h(\phi)^\top u \quad (8)$$

with u the leaky integral controller defined in (6). This *inversion dynamics* has two special properties. First, it satisfies the conditions of Theorem 2 by construction (c.f. Section S2.3). Second, as defined above, $\dot{\psi}$ resembles the second-phase dynamics of the recurrent backpropagation algorithm (c.f. Section S3). Intuitively, in this case we find an optimally-controlled equilibrium by *simultaneously* (in a single phase) running the first- and second-phase dynamics of recurrent backpropagation, with the critical difference that here the dynamical equations of both phases interact through the relation $\dot{\phi} = f(\phi, \theta) + \psi$.

2.3 The least-control principle solves the original learning problem

Iterating our parameter update minimizes the least-control objective $\mathcal{H}(\theta)$ and not directly the original objective of learning (1). The latter is however the objective of ultimate interest, used to measure the performance of the system after learning, when it is no longer under the influence of a controller. We now show that there is a close link between the two objectives and identify a wide range of conditions under which least-control solutions also solve the original learning problem (1).

Proposition 3 shows the intuitive result that if the optimal control is minimized to zero, the equilibria of the controlled and free dynamics coincide and hence the loss L is minimized at the free equilibrium as well (c.f. Figure 1).

Proposition 3. *Assuming L is convex on the system output y , we have that the optimal control ψ^* is equal to 0 iff. the free equilibrium ϕ^* minimizes L .*

As $\psi^* = -f(\phi^*, \theta)$, reaching $\psi^* = 0$ can only be done if the model is powerful enough to perfectly fit the controlled equilibria. We show in Proposition 4, that overparameterization, i.e., having more

parameters θ than system states ϕ , indeed helps solve the original learning problem (1). The condition $\partial_\theta f(\phi^*, \theta)$ being of full row rank, that is needed in this proposition, can only be satisfied when the dimensions satisfy $|\theta| \geq |\phi|$, with ϕ the concatenated states of all data points, hence providing another perspective on why overparameterization helps.

Proposition 4. *Assuming $L(y)$ is convex on the system output y , a local minimizer θ of the least control objective \mathcal{H} is a global minimizer of the original learning problem (1), under the sufficient condition that $\partial_\theta f(\phi^*, \theta)$ has full row rank.*

Fully minimizing the amount of control to zero is not always possible, which highlights the need to understand the relation between the least-control objective $\mathcal{H}(\theta) = \frac{1}{2}\|\psi^*\|^2$ and the loss $L(h(\phi^*))$ of the original learning problem (1). Proposition 5 shows that we can do so, as minimizing $\|\psi^*\|^2$ indirectly minimizes the loss $L(h(\phi^*))$, under some regularity and strong convexity assumptions.

Proposition 5. *If $\|f\|^2$ is μ -strongly convex, L is M -Lipschitz continuous and the minimum of L is 0, then*

$$L(h(\phi^*)) \leq \frac{\sqrt{\mu}}{\sqrt{2M}} \|\psi^*\| = \frac{\sqrt{\mu}}{\sqrt{2M}} \|f(\phi^*, \theta)\|.$$

Approximate equilibria. Our least-control theory requires the system to be at equilibrium, and that the loss is minimized at the controlled equilibrium. This is almost never the case in practice, for instance because the dynamics are run for a finite amount of time, the column space condition for Q is not perfectly satisfied, or because α is not zero in the output controller u dynamics. The update we take therefore does not strictly follow the gradient of the least-control objective $\mathcal{H}(\theta)$. We formally show in Section S2.6 that our update resulting from an approximate optimally-controlled equilibrium is close to the gradient $\nabla_\theta \mathcal{H}$. More precisely, under some regularity conditions on f , the error in the gradient estimation is upper bounded by the distance between ϕ^* and its estimate. Additionally, if we reach equilibrium but α is non-zero the update $-\partial_\theta f(\phi_*, \theta)^\top \psi_*$ follows the gradient of an objective very similar to the least-control one \mathcal{H} , under strict conditions on the feedback mapping Q .

2.4 The least-control principle as constrained energy minimization

We now provide a dual view of our least-control principle from the perspective of energy minimization. This will allow designing a second general-purpose dynamics for computing the optimal control ψ^* , and establishing a link to another principle for learning known as the free-energy principle. To arrive at an energy function, we rewrite the least-control objective (3) by substituting the constraint $\psi^* = -f(\phi^*, \theta)$ into this objective, leading to the following constrained optimization problem:

$$\phi^* = \arg \min_\phi \frac{1}{2} \|f(\phi, \theta)\|^2 \quad \text{s.t.} \quad \nabla_\phi L(h(\phi)) = 0 \quad (9)$$

The role of optimal control can therefore be reinterpreted as finding the state that is the closest to equilibrium under the free dynamics, among the states that minimize the loss function.

Next, we introduce the augmented energy $F(\phi, \theta, \beta) := \frac{1}{2} \|f(\phi, \theta)\|^2 + \beta L(h(\phi))$, which adds a nudging potential to the equilibrium energy $\|f(\phi, \theta)\|^2$, and take the *perfect control limit*, $\beta \rightarrow \infty$, where this potential dominates the energy. As we show in Section S2.5, minimizing the augmented energy with respect to the state variable ϕ leads to fulfilling our objective (9). Interestingly, when $\beta \rightarrow \infty$ and $f(\phi, \theta)$ implements a feedforward neural network, we recover the free-energy function which governs the model of Whittington and Bogacz [35], which was obtained from an entirely different route based on variational expectation maximization for a probabilistic latent variable model [36] (c.f. Section S4).

Energy-based dynamics as optimal control. We leverage this connection to design a second general-purpose dynamics that compute an optimal control, by using the gradient flow on F :

$$\dot{\phi} = -\partial_\phi f(\phi, \theta)^\top f(\phi, \theta) - \beta \partial_\phi h(\phi)^\top \nabla_y L(h(\phi)) \quad (10)$$

Here, the control ψ is implicitly contained in the dynamics of ϕ . Part of the dynamics, $-\beta \nabla_y L(h(\phi))$, plays the role of an infinitely-strong proportional controller on the system output; another part is in charge of optimally sending the teaching signal from the output back to the rest of the system. We refer to Section S2.5 for more details.

Two opposing limits: perfect control vs. weak nudging. The update $\partial_\theta f^\top f$ that we obtain in Theorem 1 has been extensively studied in the weak nudging limit $\beta \rightarrow 0$ [35, 37, 38], which sits

at the opposite end of the β -spectrum of the perfect control limit studied here. A seminal result shows that as $\beta \rightarrow 0$ the gradient $\nabla_{\theta} L(\phi^*)$ of the original objective function is recovered [24, 39]. However, this update is known to be sensitive to noise as the value of f can be very small at the weakly-nudged equilibrium [30]. Our least-control principle works at the opposite perfect control end of the spectrum ($\beta \rightarrow \infty$), and it is therefore more resistant to noise. One of our main contributions is to show that using the same update, but instead evaluated at an optimally-controlled state ϕ^* , still performs principled gradient-based optimization, however now on the least-control objective $\mathcal{H}(\theta)$.

3 Applications of the least-control principle

The least-control principle applies to a general class of dynamical systems at equilibrium. By contrast, the majority of previous work on local learning focused on designing circuits and rules tailored towards feedforward neural networks [14, 17, 23, 35, 40–44]. We now demonstrate the generality of our principle by applying it to two problems of interest in neuroscience and machine learning: equilibrium recurrent neural network learning and meta-learning. In both cases, our principle leads to activity-dependent local learning rules by leveraging Theorem 1, while making use of simple and flexible optimal controllers to feed back credit assignment information (c.f. Theorem 2). We test our learning and meta-learning systems on standard benchmarks and find that they perform competitively when compared to conventional gradient-based methods.

3.1 The least-control principle for equilibrium recurrent neural networks

A hallmark of the cortex is its lateral and feedback recurrent connectivity. While there is debate over the precise functional roles of recurrent processing, there is strong experimental evidence that these connections are not limited to transmitting learning signals and play an active role in information processing [e.g., 45–48]. We thus turn to equilibrium recurrent neural networks (RNNs) as a first application of our principle, aiming to demonstrate its applicability beyond feedforward models. From the viewpoint of machine learning, it has been shown that equilibrium RNNs are often more parameter-efficient than feedforward networks, while reaching state-of-the-art performance [3, 7, 9].

More concretely, we consider a RNN driven by a fixed input x assumed to converge to an equilibrium state [31, 32], obeying the following free dynamics (e.g. Figure 1.C):

$$\dot{\phi} = f(\phi, \theta) = -\phi + W\sigma(\phi) + Ux \quad (11)$$

with ϕ the neural activities, W the recurrent synaptic weights matrix, U the input weight matrix and σ the activation function. The learning problem consists of optimizing the network weights $\theta = \{W, U\}$ on a loss $L(D\phi^*)$ at the equilibrium activity ϕ^* . Here D is a fixed decoder matrix that selects output neurons from the network as $y = h(\phi) = D\phi$, with $D = [0 \text{ Id}]$. For improving performance, we incorporate a trained decoder matrix inside the recurrent weights W (see Section S6 for more details and derivations on RNNs). Note that when W has a lower block-diagonal structure, the equilibrium RNN corresponds to a conventional deep feedforward neural network.

We now add a control signal ψ to the dynamics (11). Theorem 1 guarantees that if the control steady state ψ_* is optimal, the following updates minimize the least-control objective $\mathcal{H}(\theta)$:

$$\Delta W = \psi_* \sigma(\phi_*)^\top, \quad \text{and} \quad \Delta U = \psi_* x^\top. \quad (12)$$

To showcase the flexibility of our principle, we use Theorem 2 to design various simple feedback circuits that compute these control signals, as we detail next.

3.1.1 A simple controller with direct linear feedback

To instantiate the least-control principle in its simplest form, we project the output controller u onto the recurrent neurons ϕ with direct linear feedback weights Q , which is a generalization of a recent feedforward network learning method [29] to equilibrium RNNs. Broadcasting output errors directly [49] may be seen as one of the simplest possible ways of avoiding the weight transport problem [11, 12, 16]. This results in the following dynamics:

$$\dot{\phi} = -\phi + W\sigma(\phi) + Ux + Qu, \quad \text{and} \quad \dot{u} = -\nabla_y L(D\phi) - \alpha u \quad (13)$$

with u a simple leaky integral output controller (c.f. Section 2.2), and $\nabla_y L$ the output error.

Theorem 2 guarantees that Qu_* is an optimal control in the limit of $\alpha \rightarrow 0$, if the feedback weights Q satisfy the column space condition $\text{col}[Q] = \text{row}[D(\text{Id} - W\partial_\phi\sigma(\phi_*))^{-1}]$ for all data samples. For a linear feedback mapping, this condition cannot be exactly satisfied for multiple samples as the row space is data-dependent, whereas Q is not. Still, we learn the feedback weights Q to approximately satisfy this column space condition, by using a local Hebbian rule that operates simultaneously to the learning of the other weights, inspired by recent work on feedforward networks [29, 50] (details in Section S6). The resulting update provably finds feedback weights Q that satisfy the column space condition for one sample, and we empirically verify that the control signal it gives in the multiple samples regime is close to optimal (c.f. Section S6).

Despite the simplicity of this linear feedback controller, we show that the training procedure described above is still powerful enough to learn an equilibrium RNN with a fully-connected recurrent layer of 256 neurons on the MNIST digit classification task [51] (c.f. Table 1). Notably, it performs almost as well as recurrent backpropagation (RBP), the current method of choice for equilibrium RNN training. We use fixed point iterations to find the steady states ϕ_* and u_* in Eq. (13) for computational efficiency (c.f. Section S6 for more simulation details). We also observe that the empirical performance improves by changing the parameter updates to $\Delta W = \partial_\phi\sigma(\phi_*)Qu_*\sigma(\phi_*)^\top$ and $\Delta U = \partial_\phi\sigma(\phi_*)Qu_*x^\top$ when the column space condition is not perfectly satisfied, corroborating the findings of Meulemans et al. [29, 50] in feedforward neural networks.

Method	Test accuracy
LCP - LF	97.45 \pm 0.04
LCP - DI	97.55 \pm 0.07
LCP - DI (KP)	97.47 \pm 0.19
RBP	97.67 \pm 0.03

Table 1: Classification accuracy (%) on the MNIST test set, of an equilibrium RNN (recurrent layer of 256 neurons) trained by recurrent backpropagation (RBP) and with the least-control principle (LCP) with different feedback controllers: linear feedback (LF), dynamic inversion (DI) and with learnt feedback weights (DI-KP). The reported mean \pm std is computed over 3 seeds.

3.1.2 Learning an RNN with general-purpose optimal control dynamics

In the previous section we designed and tested a simple error broadcast circuit and showed that we can learn it such that the conditions of Theorem 2 are approximately met. This approximate feedback is likely insufficient for more complex tasks which require harnessing depth or strongly-recurrent dynamics [52]. This leads us to consider two feedback circuits with more detailed architectures, which have the capacity to steer the network to an (exact) optimally-controlled equilibrium.

The first circuit is based on our general-purpose dynamic inversion (8). Applied to our RNN it yields:

$$\dot{\phi} = -\phi + W\sigma(\phi) + Ux + \psi, \quad \text{and} \quad \dot{\psi} = -\psi + \partial_\phi\sigma(\phi)S\psi + D^\top u. \quad (14)$$

The second circuit exploits the dual energy minimization view of our principle presented in Section 2.4. Taking the energy-descending dynamics $\dot{\phi} = -\partial_\phi F(\phi, \theta, \beta)^\top$ of Eq. 10, we obtain

$$\dot{\phi} = -\psi + \partial_\phi\sigma(\phi)S\psi + D^\top u, \quad \text{and} \quad \psi = \phi - W\sigma(\phi) - Ux, \quad (15)$$

where we use the output controller u of Eq. 6 as a generalization of the proportional control $-\beta\nabla_y L$ to make the two circuits more directly comparable. Above, we introduce decoupled feedback weights S to avoid sharing weights between ϕ and ψ , and we learn S to align with W^\top by using the Kolen-Pollack local learning rule [41, 53], which simply transposes the weight update ΔW (12) and adds weight decay to both update rules: $\Delta S = \sigma(\phi_*)\psi_*^\top - \gamma S$. We use D^\top in the circuits above, a weak form of weight-sharing; since D is a fixed (all-or-none weights) selector this simply amounts to assuming that the output controller u knows which neurons are the output neurons.

Both circuits implement optimal control through neural dynamics, avoiding explicit matrix inverses and phases. In biological terms, they lead to different interpretations and implementation possibilities, highlighting the flexibility of our learning principle. The dynamic inversion circuit (14) fits naturally with dendritic error implementations, where ψ can be linked to feedback dendritic compartments whose signals steer plasticity [14, 17, 20, 23, 29, 40, 50, 54]. In particular, by leveraging burst-multiplexing circuits [14, 23] or interneuron microcircuits [17], all information for the dynamics and weight updates can be made locally available (cf. Section S6). On the other hand, the energy-minimizing dynamics (15) naturally leads to an implementation based on prediction and error neuron populations, characteristic of predictive coding circuits [35, 55–57]. We provide a high-level

discussion of the two circuit alternatives (14, 15) in Section S6. In our simulations we focus on the former, but we do not expect major differences in practice between the two, as they have the same equilibrium.

We test our optimally-controlled RNNs by training a fully-connected equilibrium RNN on MNIST with circuit (14), while varying the recurrent layer width, cf. Figure 2. This analysis shows that our theoretical results of Section 2.3 translate to practice, as for strongly overparameterized networks, both \mathcal{H} and L are minimized to zero, whereas for underparameterized networks, minimizing the least-control objective $\mathcal{H}(\theta)$ leads to a significant decrease in L . Moreover, our networks achieve competitive test performance compared to RBP, both when the feedback weights are trained (LCP-DI KP) and when they are tied ($S = W^T$; LCP-DI), cf. Table 1.

Next, we test whether the circuits and rules obtained through our principle scale to more complex recurrent architectures and tasks. More concretely, we learn a recurrent block of convolutions that includes cross-sample normalization [9] on the CIFAR-10 image classification benchmark [59]. This kind of network can be interpreted as an efficient infinite-depth residual neural network with weight-sharing [60, 61]. We show on Table 2 that our system is able to match RBP, even though the models considered here are not overparametrized enough to not need control (c.f. Section S6). Lastly, we turn to implicit neural representations [62], yet another task for which recurrent connections are known to be particularly beneficial [10]. The network there has to represent an image in its weights so that it is able to map pixel coordinates with its color value. We find that our principle still performs competitively to RBP and refer to Section S6 for more details.

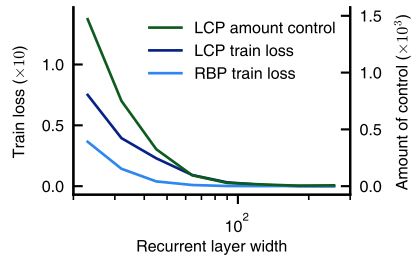


Figure 2: Training loss L and the amount of control $\|\psi^*\| = \sqrt{2\mathcal{H}}$ after training until convergence on MNIST with various recurrent layer widths.

3.2 The least-control principle for meta-learning

The generality of the least-control principle enables considering learning paradigms other than supervised learning. Here, we show that it can be applied to meta-learning, a framework that aims at improving a learning algorithm by leveraging shared structure in encountered tasks [63]. This framework is gaining traction in neuroscience, having been featured in recent work aiming at understanding which systems [64–66] and rules [30] could support meta-learning in the brain.

Meta-learning complex synapses. Following [30, 67], we model the learning algorithm for training a neural network with synaptic weights ϕ on some task τ as the minimization of a data-driven loss $L_\tau^{\text{train}}(\phi)$, regularized by a quadratic term $\lambda\|\phi - \omega\|^2$. This regularizer can be interpreted as a model of a complex synapse; similar models have been introduced in studies of continual learning and long-term memory [68–72]. In the context of meta-learning, the fast weights ϕ quickly learn how to solve a task and λ determines how strongly ϕ is pulled towards the slow weights ω , which consolidate the knowledge that has been previously acquired. The capabilities of the learning algorithm are measured by evaluating $L_\tau^{\text{eval}}(\phi_\tau^*)$, the performance of the learned neural network on data from task τ that was held out during learning. Meta-learning finally corresponds to improving the learning performance on many tasks by adjusting the meta-parameters $\theta = \omega$, leading to the following problem:

$$\min_{\theta} \mathbb{E}_{\tau} [L_{\tau}^{\text{eval}}(\phi_{\tau}^*)] \quad \text{s.t.} \quad \phi_{\tau}^* = \arg \min_{\phi} L_{\tau}^{\text{learn}}(\phi) + \frac{\lambda}{2} \|\phi - \omega\|^2. \quad (16)$$

Above, the parameters ϕ no longer represent neural activities and θ synaptic weights as in the previous section; ϕ and $\theta = \omega$ now designate synaptic weights and meta-parameters, respectively.

Method	CIFAR-10	INR
RBP	80.14 \pm 0.20	25.47 \pm 4.16
LCP-DI	80.26 \pm 0.17	25.11 \pm 2.90

Table 2: (Left) Test accuracy (%) on CIFAR-10 of a convolutional equilibrium RNN. (Right) The peak signal-to-noise ratio (in dB) of an implicit neural representation (INR) learned on a natural image dataset [58]. Mean \pm std computed over 3 seeds (CIFAR-10) and 16 images (INR).

Meta-parameter updates. Using the first-order conditions $-\nabla_{\phi} L_{\tau}^{\text{train}}(\phi_{\tau}^*) - \lambda(\phi_{\tau}^* - \theta) = 0$ associated to ϕ_{τ}^* being a minimizer in the previous equation yields an optimization problem on which the least-control principle can be applied. Our principle prescribes running the controlled dynamics

$$\begin{aligned}\dot{\phi} &= -\nabla_{\phi} L_{\tau}^{\text{learn}}(\phi) - \lambda(\phi - \omega) + u, \\ \dot{u} &= -\alpha u - \nabla_{\phi} L_{\tau}^{\text{eval}}(\phi)\end{aligned}\quad (17)$$

or any other process that finds the same fixed points $(\phi_{\tau}^*, u_{\tau}^*)$. The theory we developed in Section 2.2 guarantees that u_{τ}^* is an optimal control as long as $\alpha \rightarrow 0$ and the Hessian of the evaluation loss $\partial_{\phi}^2 L_{\tau}^{\text{eval}}$ evaluated at the equilibrium ϕ_{τ}^* is invertible. Hence, we do not need complex dynamics to compute the gradient, highlighting the flexibility and simplicity of learning according to the least-control principle. The resulting single-phase meta-learning rule is local to every synapse (c.f. Section S7):

$$\Delta\omega = \lambda u_{\tau}^{\top}. \quad (18)$$

Experimental results. Our meta-learning algorithm stands out from competing methods as being both principled, first-order and single-phase. Existing first-order and single-phase methods either approximate meta-gradients (e.g., FOMAML [73] and T1-T2 [74]) or rely on heuristics (e.g. Reptile [75]), and therefore do not provably minimize a meta-objective function. By contrast, stochastic meta-gradient descent methods require two phases to backpropagate through learning [73], invert an intractable Hessian [67, 76], or learn a slightly modified task [30], and often require second derivatives [67, 73, 76]. We compare our meta-learning rule to competing first-order methods (FOMAML, T1-T2 and Reptile) and iMAML [67] on the Omniglot few-shot visual classification benchmark [77] to show that our principled approach results in greater performance. Each Omniglot task consists of distinguishing 20 classes after seeing only 1 sample per class; we choose this 20-way 1-shot regime as the gap between first- and second-order methods is reputedly the largest compared to other variants of this benchmark. We find that our meta-learning rule significantly outperforms other first-order methods, while still lagging behind iMAML, a second-order and two-phased method. These findings are particularly interesting since our synaptic model (16) is in the underparameterized regime: there is a separate set of weights ϕ_{τ} per task τ but only one set of consolidated weights ω for the whole task distribution. The good performance observed here demonstrates that least-control solutions can perform well even when overparameterization arguments (cf. Section 2.3) do not hold.

4 Discussion

Control theories of neural network learning. The relationship between control theory and neural network learning is an old and intricate one. It is by now well known that backpropagation, the method of choice for computing gradients in deep learning, can be seen as the discrete-time counterpart of the adjoint method developed in control theory for continuous-time systems [78, 79]. One of the early papers realizing this connection formulated neural network learning as an optimization problem under equilibrium constraints, as in the original problem statement (1), and rederived the recurrent backpropagation algorithm [80]. More recent work has explored using feedback neural control circuits which influence the neural dynamics of feedforward [29, 50] and recurrent [81–83] networks to deliver learning signals. Different from such approaches, our least-control principle is rooted in *optimal* control: instead of setting the control from an ansatz, we derived it from first principles. This allowed us to arrive at a simple local rule for gradient-based learning, and to identify general sufficient conditions for the feedback control signals.

Predictive coding from the least-control perspective. We have shown that least-control problems correspond to free-energy minimization problems. This dual view of least-control problems allows connecting to influential theories of neural information processing based on predictive coding [19, 35, 36, 55, 57]. Our results elucidate predictive coding theories in at least three ways. First, Theorem 1 justifies the parameter update taken in supervised predictive coding networks [35] as gradient-based optimization of our least-control objective. Previous arguments for gradient-based learning were only known for the weak nudging limit ($\beta \rightarrow 0$) where learning signals are vanishingly

Method	Test accuracy
FOMAML [73]	89.40 \pm 0.50
T1-T2 [74]	89.72 \pm 0.43
Reptile [75]	89.43 \pm 0.14
LCP (ours)	91.00 \pm 0.24
iMAML [67]	94.46 \pm 0.42

Table 3: Omniglot character 20-way 1-shot few-shot learning. Test set classification accuracy (%) averaged over 3 seeds \pm std.

small [24], which is problematic in noisy systems such as the cortex [84]; our novel theoretical and experimental findings characterize the opposite perfect control ($\beta \rightarrow \infty$) end of the spectrum. Second, Theorem 2 broadens the class of neural network circuits which may be used to implement predictive coding, beyond the precisely-constructed microcircuits that have been proposed so far [17, 35]. Finally, our experiments on recurrent neural networks using free-energy-minimizing dynamics to assign credit are to the best of our knowledge the first of the kind, and serve to validate the effectiveness of predictive coding circuits beyond feedforward architectures.

Limitations. A limiting factor of our theory is that in its current form it is only applicable to equilibrium systems. While the study of neural dynamics at equilibrium is an old endeavor in neuroscience and neural network theory [85, 86], it remains unclear how strong an assumption it is when modeling the networks of the brain. Extending the least-control principle that we present here to out-of-equilibrium dynamical systems is an exciting direction for future work. Another limitation concerning the breadth of problem (1) is that we did not allow the loss function L to directly depend on the parameters θ . We discuss extensions to this more general case in Section S2.2, however not all loss functions L in this more general class satisfy the conditions needed to obtain a local parameter update.

Concluding remarks. We have presented a new theory that enables learning equilibrium systems with local gradient-based rules. Our learning rules are driven by changes in activity generated by an optimal control, in charge of feeding back credit assignment information into the system as it evolves. Taken together, our results push the boundaries of what is possible with single-phase, activity-dependent local learning rules, and suggest an alternative to direct gradient-based learning which yields high performance in practice.

Acknowledgments and Disclosure of Funding

This research was supported by an Ambizione grant (PZ00P3_186027) from the Swiss National Science Foundation and an ETH Research Grant (ETH-23 21-1) awarded to João Sacramento. Seijin Kobayashi was supported by the Swiss National Science Foundation (SNF) grant CRSII5_173721. Johannes von Oswald was funded by the Swiss Data Science Center (J.v.O. P18-03). We thank Angelika Steger, Benjamin Scellier, Walter Senn, Il Memming Park, Blake A. Richards, Rafal Bogacz, and members of the Senn and Bogacz labs for discussions.

References

- [1] D. J. Felleman and D. C. van Essen. Distributed hierarchical processing in the primate cerebral cortex. *Cerebral Cortex*, 1(1):1–47, 1991.
- [2] Rodney J. Douglas and Kevan A.C. Martin. Neuronal circuits of the neocortex. *Annual Review of Neuroscience*, 27(1):419–451, 2004.
- [3] Qianli Liao and Tomaso Poggio. Bridging the gaps between residual learning, recurrent neural networks and visual cortex. *arXiv preprint arXiv:1604.03640*, 2016.
- [4] Aran Nayebi, Daniel Bear, Jonas Kubilius, Kohitij Kar, Surya Ganguli, David Sussillo, James J. DiCarlo, and Daniel L. Yamins. Task-driven convolutional recurrent models of the visual system. *Advances in Neural Information Processing Systems*, 31, 2018.
- [5] Jonas Kubilius, Martin Schrimpf, Kohitij Kar, Rishi Rajalingham, Ha Hong, Najib Majaj, Elias Issa, Pouya Bashivan, Jonathan Prescott-Roy, Kailyn Schmidt, Aran Nayebi, Daniel Bear, Daniel L. Yamins, and James J. DiCarlo. Brain-like object recognition with high-performing shallow recurrent ANNs. In *Advances in Neural Information Processing Systems*, 2019.
- [6] Ruben S. van Bergen and Nikolaus Kriegeskorte. Going in circles is the way forward: the role of recurrence in visual inference. *Current Opinion in Neurobiology*, 65:176–193, 2020.
- [7] Drew Linsley, Alekh Karkada Ashok, Lakshmi Narasimhan Govindarajan, Rex Liu, and Thomas Serre. Stable and expressive recurrent vision models. In *Advances in Neural Information Processing Systems*, 2020.

- [8] Shaojie Bai, J. Zico Kolter, and Vladlen Koltun. Deep equilibrium models. *Advances in Neural Information Processing Systems*, 2019.
- [9] Shaojie Bai, Vladlen Koltun, and J. Zico Kolter. Multiscale deep equilibrium models. *Advances in Neural Information Processing Systems*, 2020.
- [10] Zhichun Huang, Shaojie Bai, and J. Zico Kolter. Implicit²: implicit layers for implicit representations. In *Advances in Neural Information Processing Systems*, 2021.
- [11] Stephen Grossberg. Competitive learning: From interactive activation to adaptive resonance. *Cognitive science*, 11(1):23–63, 1987.
- [12] Francis Crick. The recent excitement about neural networks. *Nature*, 337:129–132, 1989.
- [13] Timothy P. Lillicrap and Adam Santoro. Backpropagation through time and the brain. *Current Opinion in Neurobiology*, 55:82–89, 2019.
- [14] Konrad P. Körding and Peter König. Supervised and unsupervised learning with two sites of synaptic integration. *Journal of Computational Neuroscience*, 11(3):207–215, 2001.
- [15] Dong-Hyun Lee, Saizheng Zhang, Asja Fischer, and Yoshua Bengio. Difference target propagation. In *Joint European Conference on Machine Learning and Knowledge Discovery in Databases*, 2015.
- [16] Timothy P. Lillicrap, Daniel Cownden, Douglas B. Tweed, and Colin J. Akerman. Random synaptic feedback weights support error backpropagation for deep learning. *Nature Communications*, 7(1):13276, 2016.
- [17] João Sacramento, Rui P. Costa, Yoshua Bengio, and Walter Senn. Dendritic cortical microcircuits approximate the backpropagation algorithm. In *Advances in Neural Information Processing Systems*, 2018.
- [18] Pieter R. Roelfsema and Anthony Holtmaat. Control of synaptic plasticity in deep cortical networks. *Nature Reviews Neuroscience*, 19(3):166–180, 2018.
- [19] James C. R. Whittington and Rafal Bogacz. Theories of error back-propagation in the brain. *Trends in Cognitive Sciences*, 23(3):235–250, 2019.
- [20] Blake A. Richards and Timothy P. Lillicrap. Dendritic solutions to the credit assignment problem. *Current Opinion in Neurobiology*, 54:28–36, 2019.
- [21] Blake A. Richards, Timothy P. Lillicrap, Philippe Beaudoin, Yoshua Bengio, Rafal Bogacz, Amelia Christensen, Claudia Clopath, Rui Ponte Costa, Archy de Berker, Surya Ganguli, Colleen J. Gillon, Danijar Hafner, Adam Kepecs, Nikolaus Kriegeskorte, Peter Latham, Grace W. Lindsay, Kenneth D. Miller, Richard Naud, Christopher C. Pack, Panayiota Poirazi, Pieter Roelfsema, João Sacramento, Andrew Saxe, Benjamin Scellier, Anna C. Schapiro, Walter Senn, Greg Wayne, Daniel Yamins, Friedemann Zenke, Joel Zylberberg, Denis Therien, and Konrad P. Körding. A deep learning framework for neuroscience. *Nature Neuroscience*, 22(11):1761–1770, 2019.
- [22] Timothy P. Lillicrap, Adam Santoro, Luke Marris, Colin J. Akerman, and Geoffrey Hinton. Backpropagation and the brain. *Nature Reviews Neuroscience*, 21(6):335–346, 2020.
- [23] Alexandre Payeur, Jordan Guerguiev, Friedemann Zenke, Blake A. Richards, and Richard Naud. Burst-dependent synaptic plasticity can coordinate learning in hierarchical circuits. *Nature Neuroscience*, 24(7):1010–1019, 2021.
- [24] Benjamin Scellier and Yoshua Bengio. Equilibrium propagation: bridging the gap between energy-based models and backpropagation. *Frontiers in Computational Neuroscience*, 11, 2017.
- [25] Guillaume Bellec, Franz Scherr, Anand Subramoney, Elias Hajek, Darjan Salaj, Robert Legenstein, and Wolfgang Maass. A solution to the learning dilemma for recurrent networks of spiking neurons. *Nature Communications*, 11(1):3625, 2020.

- [26] Brandon Amos. *Differentiable optimization-based modeling for machine learning*. PhD Thesis, Carnegie Mellon University, 2019.
- [27] Stephen Gould, Richard Hartley, and Dylan John Campbell. Deep declarative networks. *IEEE Transactions on Pattern Analysis and Machine Intelligence*, 2021.
- [28] Laurent El Ghaoui, Fangda Gu, Bertrand Travacca, Armin Askari, and Alicia Tsai. Implicit deep learning. *SIAM Journal on Mathematics of Data Science*, 3(3):930–958, 2021.
- [29] Alexander Meulemans, Matilde Tristany Farinha, Maria R. Cervera, João Sacramento, and Benjamin F. Grewe. Minimizing control for credit assignment with strong feedback. *arXiv preprint arXiv:2204.07249*, 2022.
- [30] Nicolas Zuchet, Simon Schug, Johannes von Oswald, Dominic Zhao, and João Sacramento. A contrastive rule for meta-learning. *arXiv preprint arXiv:2104.01677*, 2021.
- [31] Luís B. Almeida. Backpropagation in perceptrons with feedback. In Rolf Eckmiller and Christoph v.d. Malsburg, editors, *Neural Computers*, pages 199–208. Springer Berlin Heidelberg, 1989.
- [32] Fernando J. Pineda. Recurrent backpropagation and the dynamical approach to adaptive neural computation. *Neural Computation*, 1(2):161–172, 1989.
- [33] Paul Werbos. *Beyond regression: new tools for prediction and analysis in the behavioral sciences*. Ph.D. thesis, Harvard University, 1974.
- [34] David E. Rumelhart, Geoffrey E. Hinton, and Ronald J. Williams. Learning representations by back-propagating errors. *Nature*, 323(6088):533–536, 1986.
- [35] James C. R. Whittington and Rafal Bogacz. An approximation of the error backpropagation algorithm in a predictive coding network with local Hebbian synaptic plasticity. *Neural Computation*, 29(5):1229–1262, 2017.
- [36] Karl Friston. The free-energy principle: a rough guide to the brain? *Trends in Cognitive Sciences*, 13(7):293–301, 2009.
- [37] Miguel Carreira-Perpinan and Weiran Wang. Distributed optimization of deeply nested systems. In *Artificial Intelligence and Statistics*, 2014.
- [38] Dominik Dold, Akos F. Kungl, João Sacramento, Mihai A. Petrovici, Kaspar Schindler, Jonathan Binas, Yoshua Bengio, and Walter Senn. Lagrangian dynamics of dendritic microcircuits enables real-time backpropagation of errors. In *Computational and Systems Neuroscience (Cosyne)*, 2019.
- [39] Benjamin Scellier. *A deep learning theory for neural networks grounded in physics*. PhD Thesis, Université de Montréal, 2021.
- [40] Jordan Guerguiev, Timothy P. Lillicrap, and Blake A. Richards. Towards deep learning with segregated dendrites. *eLife*, 6:e22901, 2017.
- [41] Mohamed Akrouf, Collin Wilson, Peter Humphreys, Timothy P. Lillicrap, and Douglas B. Tweed. Deep learning without weight transport. In *Advances in Neural Information Processing Systems*, 2019.
- [42] Alexander Meulemans, Francesco Carzaniga, Johan Suykens, João Sacramento, and Benjamin F. Grewe. A theoretical framework for target propagation. In *Advances in Neural Information Processing Systems*, 2020.
- [43] William F. Podlaski and Christian K. Machens. Biological credit assignment through dynamic inversion of feedforward networks. In *Advances in Neural Information Processing Systems*, 2020.
- [44] Isabella Pozzi, Sander Bohte, and Pieter Roelfsema. Attention-gated brain propagation: how the brain can implement reward-based error backpropagation. *Advances in Neural Information Processing Systems*, pages 2516–2526, 2020.

- [45] Charles D. Gilbert and Wu Li. Top-down influences on visual processing. *Nature Reviews Neuroscience*, 14(5):350–363, 2013.
- [46] Satoshi Manita, Takayuki Suzuki, Chihiro Homma, Takashi Matsumoto, Maya Odagawa, Kazuyuki Yamada, Keisuke Ota, Chie Matsubara, Ayumu Inutsuka, Masaaki Sato, Masamichi Ohkura, Akihiro Yamanaka, Yuchio Yanagawa, Junichi Nakai, Yasunori Hayashi, Matthew E. Larkum, and Masanori Murayama. A top-down cortical circuit for accurate sensory perception. *Neuron*, 86(5):1304–1316, 2015.
- [47] Tiago Marques, Julia Nguyen, Gabriela Fioreze, and Leopoldo Petreanu. The functional organization of cortical feedback inputs to primary visual cortex. *Nature Neuroscience*, 21(5):757–764, 2018.
- [48] Lisa Kirchberger, Sreedeeep Mukherjee, Ulf H. Schnabel, Enny H. van Beest, Areg Barsegyan, Christiaan N. Levelt, J. Alexander Heimel, Jeannette A. M. Lorteije, Chris van der Togt, Matthew W. Self, and Pieter R. Roelfsema. The essential role of recurrent processing for figure-ground perception in mice. *Science Advances*, 7(27):eabe1833, 2021.
- [49] Arild Nøklund. Direct feedback alignment provides learning in deep neural networks. In *Advances in Neural Information Processing Systems*, 2016.
- [50] Alexander Meulemans, Matilde Tristany Farinha, Javier Garcia Ordonez, Pau Vilimelis Aceituno, João Sacramento, and Benjamin F. Grewe. Credit assignment in neural networks through deep feedback control. In *Advances in Neural Information Processing Systems*, 2021.
- [51] Yann LeCun. The MNIST database of handwritten digits. Available at <http://yann.lecun.com/exdb/mnist>, 1998.
- [52] Sergey Bartunov, Adam Santoro, Blake Richards, Luke Marris, Geoffrey E. Hinton, and Timothy P. Lillicrap. Assessing the scalability of biologically-motivated deep learning algorithms and architectures. In *Advances in neural information processing systems*, 2018.
- [53] John F. Kolen and Jordan B. Pollack. Back-propagation without weight transport. In *Proceedings of 1994 IEEE International Conference on Neural Networks (ICNN'94)*, 1994.
- [54] Fabian A. Mikulasch, Lucas Rudelt, Michael Wibral, and Viola Priesemann. Dendritic predictive coding: A theory of cortical computation with spiking neurons. *arXiv preprint arXiv:2205.05303*, 2022.
- [55] Rajesh P. N. Rao and Dana H. Ballard. Predictive coding in the visual cortex: a functional interpretation of some extra-classical receptive-field effects. *Nature Neuroscience*, 2(1):79–87, 1999.
- [56] Andre M. Bastos, W. Martin Usrey, Rick A. Adams, George R. Mangun, Pascal Fries, and Karl J. Friston. Canonical microcircuits for predictive coding. *Neuron*, 76(4):695–711, 2012.
- [57] Georg B. Keller and Thomas D. Mrsic-Flogel. Predictive processing: a canonical cortical computation. *Neuron*, 100(2):424–435, 2018.
- [58] Rizal Fathony, Anit Kumar Sahu, Devin Willmott, and J. Zico Kolter. Multiplicative filter networks. September 2020.
- [59] Alex Krizhevsky and Geoffrey Hinton. Learning multiple layers of features from tiny images. Technical report, 2009.
- [60] Kaiming He, Xiangyu Zhang, Shaoqing Ren, and Jian Sun. Deep residual learning for image recognition. In *Proceedings of the IEEE Conference on Computer Vision and Pattern Recognition*, 2016.
- [61] Ricky T. Q. Chen, Yulia Rubanova, Jesse Bettencourt, and David K. Duvenaud. Neural ordinary differential equations. In *Advances in Neural Information Processing Systems*, 2018.

- [62] Vincent Sitzmann, Julien Martel, Alexander Bergman, David Lindell, and Gordon Wetzstein. Implicit neural representations with periodic activation functions. In *Advances in Neural Information Processing Systems*, 2020.
- [63] Sebastian Thrun and Lorien Pratt. *Learning to learn*. Springer US, 1998.
- [64] Timothy E. J. Behrens, Timothy H Muller, James C. R. Whittington, Shirley Mark, Alon B. Baram, Kimberly L Stachenfeld, and Zeb Kurth-Nelson. What is a cognitive map? Organizing knowledge for flexible behavior. *Neuron*, 100(2):490–509, 2018.
- [65] Jane X. Wang, Zeb Kurth-Nelson, Dharshan Kumaran, Dhruva Tirumala, Hubert Soyer, Joel Z. Leibo, Demis Hassabis, and Matthew Botvinick. Prefrontal cortex as a meta-reinforcement learning system. *Nature Neuroscience*, 21(6):860–868, 2018.
- [66] Jane X. Wang. Meta-learning in natural and artificial intelligence. *Current Opinion in Behavioral Sciences*, 38:90–95, 2021.
- [67] Aravind Rajeswaran, Chelsea Finn, Sham Kakade, and Sergey Levine. Meta-learning with implicit gradients. In *Advances in Neural Information Processing Systems*, 2019.
- [68] Stefano Fusi, Patrick J. Drew, and Larry F. Abbott. Cascade models of synaptically stored memories. *Neuron*, 45(4):599–611, 2005.
- [69] Lorric Ziegler, Friedemann Zenke, David B. Kastner, and Wulfram Gerstner. Synaptic consolidation: from synapses to behavioral modeling. *Journal of Neuroscience*, 35(3):1319–1334, 2015.
- [70] Marcus K. Benna and Stefano Fusi. Computational principles of synaptic memory consolidation. *Nature Neuroscience*, 19(12):1697–1706, 2016.
- [71] Friedemann Zenke, Ben Poole, and Surya Ganguli. Continual learning through synaptic intelligence. In *International Conference on Machine Learning*, 2017.
- [72] James Kirkpatrick, Razvan Pascanu, Neil Rabinowitz, Joel Veness, Guillaume Desjardins, Andrei A. Rusu, Kieran Milan, John Quan, Tiago Ramalho, Agnieszka Grabska-Barwinska, Demis Hassabis, Claudia Clopath, Dharshan Kumaran, and Raia Hadsell. Overcoming catastrophic forgetting in neural networks. *Proceedings of the National Academy of Sciences of the United States of America*, 114(13):3521–3526, 2017.
- [73] Chelsea Finn, Pieter Abbeel, and Sergey Levine. Model-agnostic meta-learning for fast adaptation of deep networks. In *International Conference on Machine Learning*, 2017.
- [74] Jelena Luketina, Mathias Berglund, Klaus Greff, and Tapani Raiko. Scalable gradient-based tuning of continuous regularization hyperparameters. In *International Conference on Machine Learning*, 2016.
- [75] Alex Nichol, Joshua Achiam, and John Schulman. On first-order meta-learning algorithms. *arXiv preprint arXiv:1803.02999*, 2018.
- [76] Jonathan Lorraine, Paul Vicol, and David Duvenaud. Optimizing millions of hyperparameters by implicit differentiation. In *International Conference on Artificial Intelligence and Statistics*, 2020.
- [77] Brenden M. Lake, Ruslan Salakhutdinov, and Joshua B. Tenenbaum. Human-level concept learning through probabilistic program induction. *Science*, 350(6266):1332–1338, 2015.
- [78] A. E. Bryson and Y. C. Ho. *Applied optimal control: optimization, estimation, and control*. Blaisdell Pub. Co., 1969.
- [79] Atilim Gunes Baydin, Barak A. Pearlmutter, Alexey Andreyevich Radul, and Jeffrey Mark Siskind. Automatic differentiation in machine learning: a survey. *Journal of Machine Learning Research*, 18:1–43, 2018.
- [80] Yann LeCun. A theoretical framework for back-propagation. In *Proceedings of the 1998 Connectionist Models Summer School*, 1988.

- [81] Aditya Gilra and Wulfram Gerstner. Predicting non-linear dynamics by stable local learning in a recurrent spiking neural network. *eLife*, 6:e28295, 2017.
- [82] Sophie Denève, Alireza Alemi, and Ralph Bourdoukan. The brain as an efficient and robust adaptive learner. *Neuron*, 94(5):969–977, 2017.
- [83] Alireza Alemi, Christian Machens, Sophie Deneve, and Jean-Jacques Slotine. Learning nonlinear dynamics in efficient, balanced spiking networks using local plasticity rules. In *Proceedings of the AAAI Conference on Artificial Intelligence*, 2018.
- [84] Dmitri A. Rusakov, Leonid P. Savtchenko, and Peter E. Latham. Noisy synaptic conductance: Bug or a feature? *Trends in Neurosciences*, 43(6):363–372, 2020.
- [85] J. J. Hopfield. Neurons with graded response have collective computational properties like those of two-state neurons. *Proceedings of the National Academy of Sciences*, 81(10):3088–3092, 1984.
- [86] Michael A. Cohen and Stephen Grossberg. Absolute stability of global pattern formation and parallel memory storage by competitive neural networks. *IEEE Transactions on Systems, Man, and Cybernetics*, SMC-13(5):815–826, 1983.
- [87] Asen L. Dontchev and R. Tyrrell Rockafellar. *Implicit functions and solution mappings*. 2009.
- [88] Luisa Zintgraf, Kyriacos Shiarlis, Vitaly Kurin, Katja Hofmann, and Shimon Whiteson. Fast context adaptation via meta-learning. In *International Conference on Machine Learning*, 2019.
- [89] Kwonjoon Lee, Subhransu Maji, Avinash Ravichandran, and Stefano Soatto. Meta-learning with differentiable convex optimization. In *Proceedings of the IEEE/CVF Conference on Computer Vision and Pattern Recognition*, 2019.
- [90] Dominic Zhao, Seijin Kobayashi, João Sacramento, and Johannes von Oswald. Meta-learning via hypernetworks. In *Workshop on Meta-Learning at NeurIPS*, 2020.
- [91] Jorge Nocedal and Stephen J. Wright. *Numerical optimization*. Springer, 2006.
- [92] Dimitri P. Bertsekas. *Constrained optimization and Lagrange multiplier methods*. Academic Press, 2014.
- [93] Karl Friston, James Kilner, and Lee Harrison. A free energy principle for the brain. *Journal of Physiology-Paris*, 100(1-3):70–87, 2006.
- [94] Radford M. Neal and Geoffrey E. Hinton. A view of the EM algorithm that justifies incremental, sparse, and other variants. In *Learning in Graphical Models*, pages 355–368. Springer Netherlands, 1998.
- [95] Dimitris G. Tzikas, Aristidis C. Likas, and Nikolaos P. Galatsanos. The variational approximation for Bayesian inference. *IEEE Signal Processing Magazine*, 25(6):131–146, 2008.
- [96] Rafal Bogacz. A tutorial on the free-energy framework for modelling perception and learning. *Journal of Mathematical Psychology*, 76:198–211, 2017.
- [97] Mark S. Goldman, Albert Compte, and Xiao-Jing Wang. Neural integrator models. *Encyclopedia of Neuroscience*, pages 165–178, 2010.
- [98] Simo Särkkä and Arno Solin. *Applied Stochastic Differential Equations*. Cambridge University Press, 2019.
- [99] Tzon-Tzer Lu and Sheng-Hua Shiou. Inverses of 2×2 block matrices. *Computers & Mathematics with Applications*, 43(1):119–129, 2002.
- [100] Jeffrey C. Magee and Christine Grienberger. Synaptic plasticity forms and functions. *Annual Review of Neuroscience*, 43:95–117, 2020.
- [101] Gordon M. Shepherd. Dendrodendritic synapses: past, present, and future. *Annals of the New York Academy of Sciences*, 1170(1):215–223, 2009.

- [102] Guillaume Hennequin, Everton J. Agnes, and Tim P. Vogels. Inhibitory plasticity: balance, control, and codependence. *Annual Review of Neuroscience*, 40:557–579, 2017.
- [103] Diederik P. Kingma and Jimmy Ba. Adam: A Method for Stochastic Optimization. In *International Conference on Learning Representations*, 2015.
- [104] Ilya Loshchilov and Frank Hutter. SGDR: Stochastic Gradient Descent with Restarts. In *International Conference on Learning Representations*, 2017.
- [105] Sergey Ioffe and Christian Szegedy. Batch normalization: accelerating deep network training by reducing internal covariate shift. In *International Conference on Machine Learning*, 2015.
- [106] Yuxin Wu and Kaiming He. Group normalization. In *Proceedings of the European Conference on Computer Vision*, 2018.
- [107] Renjie Liao, Yuwen Xiong, Ethan Fetaya, Lisa Zhang, KiJung Yoon, Xaq Pitkow, Raquel Urtasun, and Richard Zemel. Reviving and improving recurrent back-propagation. In *International Conference on Machine Learning*, 2018.
- [108] Nicolas Zucchet and João Sacramento. Beyond backpropagation: implicit gradients for bilevel optimization. *arXiv preprint arXiv:2205.03076*, 2022.

Supplementary Materials

Alexander Meulemans*, Nicolas Zucchet*, Seijin Kobayashi*, Johannes von Oswald, João Sacramento

* Equal contribution.

Table of Contents

S1 Notation	2
S1.1 General notations	2
S1.2 Notations for the least-control principle in general	2
S1.3 Notations for recurrent neural networks	2
S1.4 Notations for meta-learning	3
S2 Proofs for the least-control principle	4
S2.1 Constrained optimization and Lagrange multipliers	4
S2.2 Theorem 1: first-order gradient	4
S2.3 Theorem 2: general controller dynamics	6
S2.4 Propositions 3, 4, 5: the least-control principle solves the original learning problem	7
S2.5 The least-control principle as constrained energy minimization	8
S2.6 The parameter update is robust to approximate optimal control	11
S2.7 Quick review of constrained optimization	12
S3 Implicit gradient, recurrent backpropagation and the link to the least-control principle	14
S4 On the relation between the least-control principle, free energy and predictive coding	16
S4.1 Supervised predictive coding	16
S4.2 Equivalence between the free and augmented energies	17
S4.3 Learning with teacher clamping results in gradients on the least-control objective	18
S4.4 The optimal control interpretation of predictive coding leads to flexible dynamics.	18
S4.5 Beyond feedforward neural networks.	18
S5 Remarks on the least-control principle when using multiple data points	20
S5.1 Loss defined over finite sample of data points	20
S5.2 Loss defined by expectation over an infinite inputspace	20
S6 The least-control principle for equilibrium RNNs	21
S6.1 Equilibrium recurrent neural network model specifications	21
S6.2 Deriving a local learning rule for equilibrium RNNs	22
S6.3 A controller with direct linear feedback	22
S6.4 Using general-purpose dynamics for computing an optimal control	26
S6.5 Additional experimental details	29
S7 The least-control principle for meta-learning	33
S7.1 Derivation of the meta-parameter updates	33
S7.2 Comparison to existing meta-learning algorithms	34
S7.3 Experimental details	35

S1 Notation

In this section, we provide an extensive list of the notations we use. In particular, we detail what the different quantities precisely mean for learning recurrent neural networks and for meta-learning.

S1.1 General notations

Notation	Meaning
$\frac{\partial}{\partial x} = \partial_x$	Partial derivative of a function. The derivative of a scalar function is a row vector of size $ x $.
$\frac{d}{dx} = d_x$	Total derivative of a function. The derivative of a scalar function is a row vector of size $ x $.
∇_x	Gradient of a scalar function (column vector). We have $\nabla_x \cdot = (d_x \cdot)^\top$.
\dot{x}	Time derivative of x (column vector).
$\ \cdot\ $	Euclidean (L2) norm.
\min_x	Minimum of a function with respect to x .
$\arg \min_x$	Set of x that (locally) minimize a function.
Id	Identity matrix (size defined by the context).
$\text{col}[A]$	Column space of A , that is $\text{Im}[A]$.
$\text{row}[A]$	Row space of A , that is $\text{Im}[A^\top]$.

S1.2 Notations for the least-control principle in general

Notation	Meaning
ϕ	Dynamical parameters of the system.
θ	Parameters of the system.
$f(\phi, \theta)$	Vector-field of the (free) dynamics on ϕ .
L	Learning loss that the system should minimize.
$y = h(\phi)$	Output units (i.e. units on which the loss is evaluated) of the system.
\mathcal{H}	Least-control objective.
ψ	Controller whose goal is to help the system reaching a loss-minimizing state.
u	Controller on the output units.
$Q(\phi, \theta)$	General feedback mapping from output control u to the entire system control ψ . We have $\psi = Q(\phi, \theta)u$ at equilibrium.
ϕ^*	Equilibrium of the free dynamics.
ϕ^*, ψ^*, u^*	Optimal state, control and output control according for the least-control objective (c.f. Eq. 3).
ϕ_*, ψ_*, u_*	Equilibrium of the controlled dynamics. The least-control principle aims for $\psi_* = \psi^*$, that is to find an optimal control through the steady state of controlled dynamics.
α	Leakage strength in a leaky integral controller ($\alpha = 0$ yields pure integral control).
β	Strength of the proportional control, or of nudging in the energy-based view.

S1.3 Notations for recurrent neural networks

Notation	Meaning
ϕ	Neural activities of all the neurons in the network (column vector).
$\theta = \{W, S\}$	Learnable synaptic connection weights of the network.
$f(\phi, \theta)$	Dynamics of the neural network.
$y = D\phi$	The binary matrix D selects output neurons u from the rest of them ϕ .
σ	Non-linear activation function.
x	Input of the neural network.
y^{true}	Desired output corresponding to an input x .
L	Loss measuring the discrepancy between outputs of the network y (that depends on x) and target output y^{true} , averaged over all the pairs (x, y^{true}) from a data set.
γ	Weight decay for the Kollen-Pollack learning-rule.

S1.4 Notations for meta-learning

Notation	Meaning
ϕ	Parameters (weights and biases) of the neural network that is learned.
$\theta = \{\omega, \lambda\}$	Parameters of the learning algorithm, here the consolidated synaptic weights ω , and eventually, the strength of attraction to those weights λ .
$f(\phi, \theta)$	Dynamics of the learning algorithm.
τ	Index of the task considered.
$L_{\tau}^{\text{learn}}(\phi)$	Data-driven loss that is combined with a prior-term to obtain the loss minimized by the learning algorithm.
$L_{\tau}^{\text{eval}}(\phi)$	Loss measuring the performance of the output of the learning algorithm.
$\psi = u$	Controller on all the units (they are all output units in this context).

S2 Proofs for the least-control principle

The purpose of this section is to prove all the theoretical results behind the least-control principle. Recall that our principle advocates to solve the following constrained optimization problem

$$\min_{\theta} \min_{\phi, \psi} \frac{1}{2} \|\psi\|^2 \quad \text{s.t.} \quad f(\phi, \theta) + \psi = 0, \quad \frac{\partial L}{\partial \phi}(h(\phi)) = 0, \quad (19)$$

that is minimizing the amount of control needed to reach a loss-minimizing state. Finding an optimal control ψ^* consists in solving the least-control problem:

$$(\phi^*, \psi^*) = \arg \min_{\phi, \psi} \frac{1}{2} \|\psi\|^2 \quad \text{s.t.} \quad f(\phi, \theta) + \psi = 0, \quad \frac{\partial L}{\partial \phi}(h(\phi)) = 0. \quad (20)$$

Most of the proofs that we present here rely on interpreting the problem above as a constrained minimization problem, and using the associated first-order stationarity condition to manipulate ψ^* and ϕ^* .

S2.1 Constrained optimization and Lagrange multipliers

Throughout the proofs for the least-control principle, we characterize the optimal control ψ^* and state ϕ^* through the stationarity conditions that they verify, that are known as the KKT conditions. In particular, this allows considering (ϕ^*, ψ^*) as an implicit function of θ , and computing derivatives through the implicit function theorem [87]. We provide a quick review on constrained optimization in Section S2.7 for the reader who is new to the topic.

We now state what are the KKT conditions for the constrained optimization problem (20). To do so, we introduce the corresponding Lagrangian, which we denote as the LCP-Lagrangian:

$$\mathcal{L}(\phi, \psi, \lambda, \mu, \theta) := \frac{1}{2} \|\psi\|^2 + \lambda^\top (f(\phi, \theta) + \psi) + \frac{\partial L}{\partial y}(h(\phi))\mu, \quad (21)$$

where λ and μ are the Lagrange multipliers associated to the constraints $f(\phi, \theta) + \psi = 0$ and $\nabla_y L(h(\phi)) = 0$. Then, (ϕ^*, ψ^*) verifies the KKT conditions associated to Eq. 20 if there exists (λ^*, μ^*) such that

$$\begin{cases} \frac{\partial \mathcal{L}}{\partial \phi}(\phi^*, \psi^*, \lambda^*, \mu^*, \theta) = \lambda^{*\top} \frac{\partial f}{\partial \phi}(\phi^*, \theta) + \mu^{*\top} \frac{\partial^2 L}{\partial y^2}(h(\phi^*)) \frac{\partial h}{\partial \phi}(\phi^*) = 0 \\ \frac{\partial \mathcal{L}}{\partial \psi}(\phi^*, \psi^*, \lambda^*, \mu^*, \theta) = \psi^{*\top} + \lambda^{*\top} = 0 \\ \frac{\partial \mathcal{L}}{\partial \lambda}(\phi^*, \psi^*, \lambda^*, \mu^*, \theta) = f(\phi^*, \theta)^\top + \psi^{*\top} = 0 \\ \frac{\partial \mathcal{L}}{\partial \mu}(\phi^*, \psi^*, \lambda^*, \mu^*, \theta) = \frac{\partial L}{\partial y}(h(\phi^*)) = 0. \end{cases} \quad (22)$$

In the proofs that follow, we use equivalently that (ϕ^*, ψ^*) is optimal for Eq. 20 and that it verifies the KKT conditions of Eq. 22. We need to invoke sufficient conditions, such as the positive definiteness of the Hessian of the Lagrangian, to make it rigorous and to show that a state satisfying the KKT conditions is a local minimizer; we discuss this matter in more details in Section S2.7. However, we omit these considerations in the proofs to keep the arguments as concise as possible.

S2.2 Theorem 1: first-order gradient

We first state the formal version of Theorem 1 and then prove it, by differentiating through the KKT conditions (22). Note that we provide an alternate proof that leverages the energy-based formulation of the principle in Section S2.5.

Theorem S1 (Formal). *Let (ϕ^*, ψ^*) an optimal control for the least-control problem (20) and (λ^*, μ^*) the Lagrange multipliers for which the KKT conditions are satisfied. Under the assumption that the Hessian of the LCP-Lagrangian $\partial_{\phi, \psi, \lambda, \mu}^2 \mathcal{L}(\phi^*, \psi^*, \lambda^*, \mu^*, \theta)$ is invertible, the least-control principle yields the following gradient for θ :*

$$\left(\frac{d}{d\theta} \mathcal{H}(\theta) \right)^\top = -\frac{\partial f}{\partial \theta}(\phi^*, \theta)^\top \psi^* = \frac{\partial f}{\partial \theta}(\phi^*, \theta)^\top f(\phi^*, \theta). \quad (23)$$

Proof. The proof relies on two ingredients: rewriting \mathcal{H} using the LCP-Lagrangian and then differentiating through this Lagrangian.

We start by rewriting the least-control objective $\mathcal{H}(\theta)$ using the LCP-Lagrangian. Recall that \mathcal{H} is defined as

$$\mathcal{H}(\theta) = \frac{1}{2} \|\psi^*\|^2. \quad (24)$$

As (ϕ^*, ψ^*) is an optimal control, there indeed exists Lagrange multipliers (λ^*, μ^*) such that $\partial_{\phi, \psi, \lambda, \mu} \mathcal{L}(\phi^*, \psi^*, \lambda^*, \mu^*, \theta) = 0$, as assumed in the statement of the theorem. We use this equality condition to implicitly define $(\phi^*, \psi^*, \lambda^*, \mu^*)$ as functions of θ . The implicit function theorem along with the assumption that the Hessian is invertible ensures that these functions are well defined and differentiable. As all the constraints are satisfied for (ϕ^*, ψ^*) , we have

$$\begin{aligned} \mathcal{H}(\theta) &= \mathcal{L}(\phi^*, \psi^*, \lambda^*, \mu^*, \theta) \\ &= \frac{1}{2} \|\psi^*\|^2 + \lambda^{*\top} (f(\phi^*, \theta) + \psi^*) + \frac{\partial L}{\partial y}(h(\phi^*)) \mu^* \\ &= \frac{1}{2} \|\psi^*\|^2 \end{aligned} \quad (25)$$

We can then calculate $d_\theta \mathcal{H}(\theta)$:

$$\begin{aligned} \frac{d}{d\theta} \mathcal{H}(\theta) &= \frac{d}{d\theta} \mathcal{L}(\phi^*, \psi^*, \lambda^*, \mu^*, \theta) \\ &= \frac{\partial \mathcal{L}}{\partial \theta} + \frac{\partial \mathcal{L}}{\partial \phi} \frac{d\phi^*}{d\theta} + \frac{\partial \mathcal{L}}{\partial \psi} \frac{d\psi^*}{d\theta} + \frac{\partial \mathcal{L}}{\partial \lambda} \frac{d\lambda^*}{d\theta} + \frac{\partial \mathcal{L}}{\partial \mu} \frac{d\mu^*}{d\theta} \\ &= \frac{\partial \mathcal{L}}{\partial \theta} + 0 + 0 + 0 + 0 \\ &= \lambda^{*\top} \frac{\partial f}{\partial \theta}(\phi^*, \theta), \end{aligned} \quad (26)$$

where we used the chain rule for the second equation, and the stationarity equations of the Lagrangian for the third equation. Through the stationarity equation $\partial_\psi \mathcal{L}(\phi^*, \psi^*, \lambda^*, \mu^*, \theta) = 0$, we have that $\lambda^* = -\psi^*$. The constraint on ψ additionally implies that $\psi^* = -f(\phi^*, \theta)$, which finishes the proof. \square

Extension to θ -dependent losses. Throughout this work, we focus on loss functions $L(\phi)$ that do not explicitly depend on θ . The influence of θ on the loss only appears through the equilibrium condition $f(\phi, \theta) = 0$. Still, we can generalize Theorem S1 further by also considering loss functions that explicitly depend on θ , on top of their implicit dependence on θ through ϕ . A simple example is when we add a weight regularization term $\|\theta\|^2$ to the loss L when training neural networks, or in meta-learning when θ does not only impact the learning algorithm of the system but also its prediction [88–90].

The proof of Theorem S1 can be slightly adapted to hold for the more general case, the only difference is that the equality $\partial_\theta \mathcal{L} = \lambda_*^\top \partial_\theta f(\phi_*, \theta)$ is no longer true. Instead, we have

$$\begin{aligned} \frac{d}{d\theta} \mathcal{H}(\theta) &= \frac{\partial \mathcal{L}}{\partial \theta}(\phi^*, \psi^*, \lambda^*, \mu^*, \theta) \\ &= -\psi^{*\top} \frac{\partial f}{\partial \theta}(\phi^*, \theta) + \mu^{*\top} \frac{\partial^2 L}{\partial \theta \partial y}(\phi^*, \theta). \end{aligned} \quad (27)$$

The second derivative $\partial_\theta \partial_y L(h(\phi^*), \theta)$ captures mixed dependencies of the loss L on y and θ . Note that when the loss L contains no terms mixing $h(\phi)$ and θ , as in the weight decay example we mentioned earlier, this second-order derivative is zero. As for this weight decay example the resulting updates are the same as for the loss without any weight decay, this indicates that some θ -dependent losses are not captured in the least-control principle we introduced in the main text.

We now propose an extended formulation of the least-control principle to fully incorporate θ -dependent losses:

$$\min_{\theta} \min_{\phi, \psi} \frac{1}{2} \|\psi\|^2 + L(\phi, \theta) \quad \text{s.t.} \quad f(\phi, \theta) + \psi = 0, \quad \nabla_{\phi} L(\phi, \theta) = 0. \quad (28)$$

Intuitively, the least-control objective $\|\psi\|^2$ combined with the constraint that the loss is minimized w.r.t. ϕ at the controlled equilibrium captures all the ways θ influences the loss through ϕ , and the new term $L(\phi, \theta)$ takes care of the ways in which θ influences the loss without influencing ϕ , while keeping the same stationarity conditions for the LCP-Lagrangian (the extra term $\nabla_y L(h(\phi^*), \theta)$ that now appears in $\partial_\phi \mathcal{L}$ vanishes). Using the same proof strategy as in Theorem 1, we obtain the following gradient:

$$\begin{aligned} \frac{d}{d\theta} \mathcal{H}(\theta) &= \frac{\partial \mathcal{L}}{\partial \theta}(\phi^*, \psi^*, \lambda^*, \mu^*, \theta) \\ &= -\psi^{*\top} \frac{\partial f}{\partial \theta}(\phi^*, \theta) + \mu^{*\top} \frac{\partial^2 L}{\partial \theta \partial y}(\phi^*, \theta) + \frac{\partial L}{\partial \theta}(\phi^*, \theta). \end{aligned} \quad (29)$$

This generalized least-control principle now allows to fully consider terms in the loss that depend on θ , while keeping the nice properties of being single-phased, having no need to invert any Jacobian, and using no infinitesimal learning signals. However, now the learning rule is not always first-order anymore due the mixed second-order derivative.

One special case of interest where the resulting learning rule is first-order again is when the θ -dependence of the loss is encapsulated in the decoder $h(\phi, \theta)$, i.e. when we have the loss $L(h(\phi, \theta))$. Applying Eq. 29 to this loss results in:

$$\begin{aligned} \frac{d}{d\theta} \mathcal{H}(\theta) &= -\psi^{*\top} \frac{\partial f}{\partial \theta}(\phi^*, \theta) + \mu^{*\top} \frac{\partial^2 L}{\partial y^2}(h(\phi^*, \theta)) \frac{\partial h}{\partial \theta}(\phi^*, \theta) + \frac{\partial L}{\partial y}(h(\phi^*, \theta)) \frac{\partial h}{\partial \theta}(\phi^*, \theta). \\ &= -\psi^{*\top} \frac{\partial f}{\partial \theta}(\phi^*, \theta) + \mu^{*\top} \frac{\partial^2 L}{\partial y^2}(h(\phi^*, \theta)) \frac{\partial h}{\partial \theta}(\phi^*, \theta) + 0 \end{aligned} \quad (30)$$

where the last term vanishes as $\partial_y L(h(\phi^*, \theta)) = 0$ is enforced by the constraints of the least-control objective of Eq. 3. When we use the inversion dynamics (8) or the energy-based dynamics (10), we can easily access the Lagrange multiplier μ^* . For this, let us take a look at the equilibrium equation of the inversion dynamics (8), which is equivalent to the equilibrium condition of the energy-based dynamics (10) if $\partial_\phi f(\phi^*, \theta)$ is invertible:

$$0 = \left(\frac{\partial f(\phi_*, \theta)}{\partial \phi} \right)^\top \psi_* + \frac{\partial h(\phi_*, \theta)}{\partial \phi}^\top u_* \quad (31)$$

Comparing this equilibrium condition with the KKT conditions of Eq. 22, and using the relation $\lambda^* = -\psi^*$, we have that

$$\frac{\partial^2 L(h(\phi_*, \theta))}{\partial y^2} \mu^* = -u_* \quad (32)$$

when $\partial_\phi h(\phi_*, \theta)$ is full rank and in the limit of $\alpha \rightarrow 0$ such that $(\phi_*, \psi_*) = (\phi^*, \psi^*)$. Taking everything together, we arrive at the following simple first-order update rule for models with a θ -dependent decoder h , in the limit of $\alpha \rightarrow 0$:

$$\frac{d}{d\theta} \mathcal{H}(\theta) = -\psi_*^\top \frac{\partial f}{\partial \theta}(\phi_*, \theta) - u_*^\top \frac{\partial h(\phi_*, \theta)}{\partial \theta} \quad (33)$$

Note that this update only holds when the inversion dynamics (8) or energy-based dynamics (10) are used. If other dynamics are used for finding the optimal control ψ^* , one needs to investigate case-by-case how to compute the Lagrange multiplier μ^* .

S2.3 Theorem 2: general controller dynamics

Theorem 2 shows that we can find optimal control ψ^* and state ϕ^* for Eq. 20 through dynamics exhibiting the following equilibrium equations

$$0 = f(\phi_*^\alpha, \theta) + Q(\phi_*^\alpha, \theta) u_*^\alpha \quad \text{and} \quad 0 = -\nabla_y L(h(\phi_*^\alpha)) - \alpha u_*^\alpha \quad (34)$$

in the limit $\alpha \rightarrow 0$, when $Q(\phi_*^\alpha, \theta)$ satisfies the column space condition (35). We prove that by showing that the limit satisfies the KKT conditions, and hence is optimal. We restate Theorem 2 below with the full technical specifications.

Theorem S2 (Formal). Let $(\phi_*^\alpha, u_*^\alpha)$ be a steady state of the generalized dynamics satisfying (34) such that ϕ_*^α admits a finite limit ϕ^* when α goes to 0. Assume that $\partial_\phi f(\phi^*)$ and $\partial_y^2 L(\phi^*)$ are invertible, $\partial_\phi h(\phi^*)$ is full rank, Q is continuous, and that the following column space condition is satisfied:

$$\text{col}[Q(\phi^*, \theta)] = \text{row} \left[\frac{\partial h}{\partial \phi}(\phi^*) \left(\frac{\partial f}{\partial \phi}(\phi^*, \theta) \right)^{-1} \right] \quad (35)$$

Then, u_*^α converges to a finite limit u^* and $(\phi^*, Q(\phi^*, \theta)u^*)$ verifies the KKT conditions for the least-control problem (20).

Proof. Note that there is a slight abuse of notation in the statement of the theorem as we use the superscript \star to denote the limits of the different quantities without yet knowing if they correspond to an optimal quantity for the least-control problem (20). Part of the proof is to actually show that those limits are optimal.

First, we show that u_*^α has a finite limit when α goes to 0. The function ϕ_*^α admits a finite limit ϕ^* when α goes to zero by hypothesis. Taking $\alpha \rightarrow 0$ in the equilibrium equations (34) results in

$$f(\phi^*, \theta) - \lim_{\alpha \rightarrow 0} \frac{1}{\alpha} Q(\phi_*^\alpha, \theta) \nabla_y L(h(\phi_*^\alpha)) = 0, \quad (36)$$

as f is continuous. The matrices $\partial_\phi h(\phi^*)$ and $\partial_\phi f(\phi^*, \theta)^{-1}$ are full rank, so the column space condition implies that $Q(\phi^*, \theta)$ is also full rank. We can therefore extract $Q(\phi_*^\alpha, \theta)$ out of the limit in the previous equation:

$$\lim_{\alpha \rightarrow 0} \frac{1}{\alpha} Q(\phi_*^\alpha, \theta) \nabla_y L(h(\phi_*^\alpha)) = Q(\phi^*, \theta) \lim_{\alpha \rightarrow 0} \frac{1}{\alpha} \nabla_y L(h(\phi_*^\alpha)), \quad (37)$$

so that $u_*^\alpha = -\alpha^{-1} \nabla_y L(h(\phi_*^\alpha))$ has a finite limit that we note u^* , using once again the fact that $Q(\phi^*, \theta)$ is full rank and (36). In particular, this implies that ϕ^* is feasible as $\nabla_y L(h(\phi_*^\alpha)) = O(\alpha)$ so $\nabla_y L(h(\phi^*)) = 0$.

We can now prove that the KKT conditions are satisfied at (ϕ^*, ψ^*) with $\psi^* := Q(\phi^*, \theta)u^*$. Note that we have $f(\phi^*, \theta) + \psi^* = 0$ by taking the limit $\alpha \rightarrow 0$ in the equilibrium equation

$$f(\phi_*^\alpha, \theta) - \frac{1}{\alpha} Q(\phi_*^\alpha, \theta) \nabla_y L(h(\phi_*^\alpha)) = 0. \quad (38)$$

As $\text{col}[Q(\phi^*, \theta)] = \text{row}[\partial_\phi h(\phi^*) \partial_\phi f(\phi^*, \theta)^{-1}]$, and $\partial_y^2 L(h(\phi^*))$ is invertible, there exist a μ and μ^* , such that

$$\begin{aligned} \psi^* &= Q(\phi^*, \theta)u^* \\ &= \frac{\partial f}{\partial \phi}(\phi^*, \theta)^{-\top} \frac{\partial h}{\partial \phi}(\phi^*)^\top \mu \\ &= \frac{\partial f}{\partial \phi}(\phi^*, \theta)^{-\top} \frac{\partial h}{\partial \phi}(\phi^*)^\top \frac{\partial^2 L}{\partial y^2}(\phi^*) \mu^*. \end{aligned} \quad (39)$$

Multiplying from the left with $\partial_\phi f(\phi^*, \theta)^\top$ results in

$$-\frac{\partial f}{\partial \phi}(\phi^*, \theta)^\top \psi^* + \frac{\partial h}{\partial \phi}(\phi^*)^\top \frac{\partial^2 L}{\partial y^2}(\phi^*) \mu^* = 0. \quad (40)$$

We now take $\lambda^* := -\psi^*$ and can easily check that $(\phi^*, \psi^*, \lambda^*, \mu^*)$ is a stationary point for the LCP-Lagrangian, i.e. it satisfies the KKT conditions (20). It follows that ψ^* is an optimal control and ϕ^* an optimally-controlled state. \square

S2.4 Propositions 3, 4, 5: the least-control principle solves the original learning problem

We here restate the results from Section 2.3 and prove them.

Proposition S3. Assuming L is convex on the system output y , we have that the optimal control ψ^* is equal to 0 iff. the free equilibrium ϕ^* minimizes L .

Proof. First remark that, as L is convex, ϕ being a minimizer of $L(h(\phi))$ is equivalent to $\nabla_y L(h(\phi)) = 0$. Then, the two conditions are equivalent to ϕ^* and ϕ^* satisfying both $f(\phi, \theta) = 0$ and $\nabla_y L(h(\phi)) = 0$. \square

Proposition S4. *Assuming L is convex on the system output y , a local minimizer θ of the least-control objective \mathcal{H} is a global minimizer of the original learning problem (1), under the sufficient condition that $\partial_\theta f(\phi^*, \theta)$ has full row rank.*

Proof. As θ is a local minimizer of $\mathcal{H}(\theta)$, we have that

$$\frac{d}{d\theta} \mathcal{H}(\theta) = f(\phi^*, \theta)^\top \frac{\partial f}{\partial \theta}(\phi^*, \theta) = 0. \quad (41)$$

The full row rank assumption of $\partial_\theta f(\phi^*, \theta)$ ensures that $f(\phi^*, \theta) = 0$. We hence have that ϕ^* is a global minimizer of $L(h(\phi))$, as $\nabla_y L(h(\phi^*)) = 0$, and L is convex, and satisfies $f(\phi^*, \theta) = 0$. It follows that θ is a global minimizer for the original learning problem. \square

Proposition S5. *If $\frac{1}{2}\|f\|^2$ is μ -strongly convex as a function of ϕ , $L \circ h$ is M -Lipschitz continuous and the minimum of L is 0, then*

$$L(h(\phi^*)) \leq \frac{\sqrt{\mu}}{\sqrt{2M}} \|\psi^*\| \leq \frac{\sqrt{\mu}}{\sqrt{2M}} \|f(\phi^*, \theta)\|. \quad (42)$$

Proof. As $h(\phi_*)$ minimizes L and L is Lipschitz-continuous,

$$L(h(\phi^*)) = L(h(\phi^*)) - L(h(\phi^*)) \leq M \|\phi^* - \phi^*\|. \quad (43)$$

The strong convexity of $\frac{1}{2}\|f\|^2$ yields

$$\frac{1}{2}\|f(\phi^*, \theta)\| = \frac{1}{2}\|f(\phi^*, \theta)\|^2 - \frac{1}{2}\|f(\phi^*, \theta)\|^2 \geq \frac{\mu}{2} \|\phi^* - \phi^*\|^2, \quad (44)$$

as ϕ^* is a global minimizer of $\frac{1}{2}\|f\|^2$. Gathering the last two inequalities gives the desired result. \square

We state and prove the remaining informal statements on the impact of approximate equilibria appearing in Section 2.3 in Section S2.6, as they require the energy-based view of the least control principle to be proved.

S2.5 The least-control principle as constrained energy minimization

In Section 2.4, we show that substituting the constraint $f(\phi, \theta) + \psi = 0$ back into the least-control problem implies that ϕ^* is a minimizer of

$$\min_{\phi} \frac{1}{2}\|f(\phi, \theta)\|^2 \quad \text{s.t.} \quad \nabla_y L(h(\phi)) = 0. \quad (45)$$

The same objective can be obtained from an energy-based perspective, by minimizing the augmented energy $F(\phi, \theta, \beta) = \frac{1}{2}\|f(\phi, \theta)\|^2 + \beta L(h(\phi))$ and taking the limit $\beta \rightarrow +\infty$. We formalize this result by first showing that the limit of stationary points of F when $\beta \rightarrow \infty$ satisfies the KKT conditions (Proposition S6), and that the global minimizers coincide, under more restrictive assumption (Proposition S7). Note that the KKT conditions associated to (45) are different from the ones in Eq. 22: the corresponding Lagrangian is

$$\mathcal{L}(\phi, \mu, \theta) := \frac{1}{2}\|f(\phi, \theta)\|^2 + \mu^\top (\nabla_y L(h(\phi))) \quad (46)$$

and KKT conditions are

$$\begin{cases} \frac{\partial \mathcal{L}}{\partial \phi}(\phi^*, \mu^*, \theta) = \frac{\partial}{\partial \phi} \left[\frac{1}{2}\|f(\phi^*, \theta)\|^2 \right] + \mu^{*\top} \frac{\partial^2 L}{\partial y^2}(h(\phi^*)) \frac{\partial h}{\partial \phi}(\phi^*) = 0 \\ \frac{\partial \mathcal{L}}{\partial \mu}(\phi^*, \mu^*, \theta) = \nabla_y L(h(\phi^*)) = 0 \end{cases}. \quad (47)$$

Proposition S6. Let ϕ_*^β be a function of β that admits a finite limit ϕ^* when β goes to infinity and verifies

$$\frac{\partial F}{\partial \phi}(\phi_*^\beta, \beta, \theta) = 0 \quad (48)$$

for every β . If we further assume that the loss Hessian $\partial_y^2 L(h(\phi^*))$ is invertible and $\partial_\phi h(\phi^*)$ is full rank, then ϕ^* satisfies the KKT conditions associated to Eq. 45.

Proof. We use the shorthand $E := \frac{1}{2}\|f\|^2$ for conciseness. For every β , ϕ_*^β verifies

$$\frac{\partial F}{\partial \phi}(\phi_*^\beta, \theta, \beta) = \frac{\partial E}{\partial \phi}(\phi_*^\beta, \theta) + \beta \frac{\partial L}{\partial y}(h(\phi_*^\beta)) \frac{\partial h}{\partial \phi}(\phi_*^\beta) = 0 \quad (49)$$

By taking β to infinity in the equation above and using continuity of $\partial_\phi E$, we obtain

$$\frac{\partial E}{\partial \phi}(\phi^*) = - \lim_{\beta \rightarrow \infty} \beta \frac{\partial L}{\partial y}(h(\phi_*^\beta)) \frac{\partial h}{\partial \phi}(\phi_*^\beta). \quad (50)$$

This first implies that

$$\frac{\partial L}{\partial y}(h(\phi^*)) \frac{\partial h}{\partial \phi}(\phi^*) = \lim_{\beta \rightarrow \infty} \frac{\partial L}{\partial y}(h(\phi_*^\beta)) \frac{\partial h}{\partial \phi}(\phi_*^\beta) = 0 \quad (51)$$

as $\partial_\phi h$, $\partial_y L$ and h are continuous, and then that $\nabla_y L(h(\phi^*)) = 0$ as $\partial_\phi h(\phi^*)$ is full rank.

Eq. 50, along with $\partial_\phi h(\phi^*)$ being full rank, implies that $\beta \partial_y L(h(\phi_*^\beta))$ admits a finite limit, note it μ . As $\partial_y^2 L(h(\phi^*))$ is invertible, there exists μ^* such that $\partial_y^2 L(h(\phi^*)) \mu^* = \mu$. Put back into (50) it yields

$$\frac{\partial E}{\partial \phi}(\phi^*) + \mu^{*\top} \frac{\partial^2 L}{\partial y^2}(h(\phi^*)) \frac{\partial h}{\partial \phi}(\phi^*) = 0, \quad (52)$$

hence ϕ^* satisfies the KKT conditions associated to (45). \square

Proposition S7. Assume L to positive and equal to 0 if and only if $\nabla_y L = 0$. Let ϕ_*^β be a global minimizer of the augmented energy F for every β , such that ϕ_*^β admits a finite limit ϕ^* when β goes to infinity. Then the limit ϕ^* is a global minimizer of the constrained optimization problem (45).

Proof. First, remark that the condition on the minimizers of L implies that solving

$$\min_{\phi} \frac{1}{2} \|f(\phi, \theta)\|^2 \quad \text{s.t.} \quad \nabla_y L(h(\phi)) = 0 \quad (53)$$

is equivalent to solving

$$\min_{\phi} \frac{1}{2} \|f(\phi, \theta)\|^2 \quad \text{s.t.} \quad L(h(\phi)) = 0. \quad (54)$$

We use the second characterization in the rest of the proof.

We introduce the short hand

$$f^* := \min_{\phi} \frac{1}{2} \|f(\phi, \theta)\|^2 \quad \text{s.t.} \quad L(h(\phi)) = 0. \quad (55)$$

For any ϕ we have that

$$F(\phi_*^\beta, \theta, \beta) \leq F(\phi, \theta, \beta) \quad (56)$$

by definition of ϕ_*^β , in particular for all the ϕ verifying the constraint $L(h(\phi)) = 0$. It follows that

$$F(\phi_*^\beta, \theta, \beta) \leq \min_{L(h(\phi))=0} F(\phi, \theta, \beta) = \min_{L(h(\phi))=0} \frac{1}{2} \|f(\phi, \theta)\|^2 = f^*. \quad (57)$$

The last inequality can be rewritten as

$$L(h(\phi_*^\beta)) \leq \frac{f^* - \|f(\phi_*^\beta, \theta)\|^2/2}{\beta}.$$

The upper bound converges to 0 as the numerator converges to a finite value by continuity of $\|f\|^2$. Since L is positive and continuous and h is continuous we obtain $L(h(\phi^*)) = 0$, i.e., ϕ^* is feasible.

We now show that $\|f(\phi^*, \theta)\|^2/2 = f^*$. As ϕ^* is feasible we have

$$f^* = \min_{L(h(\phi))=0} \frac{1}{2} \|f(\phi, \theta)\|^2 \leq \frac{1}{2} \|f(\phi^*, \theta)\|^2. \quad (58)$$

This implies that

$$\limsup_{\beta \rightarrow \infty} F(\phi_*^\beta, \theta, \beta) = \frac{1}{2} \|f(\phi^*, \theta)\|^2 + \limsup_{\beta \rightarrow \infty} \beta L(h(\phi_*^\beta)) \geq f^* \quad (59)$$

where we used the positivity of L for the last inequality. Because of (57), we also have

$$\limsup_{\beta \rightarrow \infty} F(\phi_*^\beta, \beta) \leq f^* \quad (60)$$

so that the combination of the last two equations yield

$$\limsup_{\beta \rightarrow \infty} \beta L(h(\phi_*^\beta)) = 0 \quad (61)$$

and

$$\frac{1}{2} \|f(\phi^*, \theta)\|^2 = f^*. \quad (62)$$

This finishes the proof. \square

Remark 1. Under the same assumptions, we can actually show that, for any $\beta, \beta' \in \mathbb{R}_+$, we have

$$0 \leq F(\phi_*^\beta, \theta, \beta) \leq F(\phi_*^{\beta'}, \theta, \beta') \leq \frac{1}{2} \|f(\phi^*, \theta)\|^2. \quad (63)$$

This can be obtained by combining Proposition S7 and the fact that $\beta \mapsto F(\phi_*^\beta, \theta, \beta)$ is a non decreasing function as

$$\begin{aligned} \frac{d}{d\beta} F(\phi_*^\beta, \theta, \beta) &= \frac{\partial F}{\partial \beta}(\phi_*^\beta, \theta, \beta) + \frac{\partial F}{\partial \phi}(\phi_*^\beta, \theta, \beta) \frac{d\phi_*^\beta}{d\beta} \\ &= L(\phi_*^\beta) + 0 \\ &\geq 0. \end{aligned} \quad (64)$$

The function $\beta \mapsto F(\phi_*^\beta, \theta, \beta)$ therefore converges to the least-control objective $\mathcal{H}(\theta)$ from below.

In the energy-based view of the least-control principle, the least-control objective becomes

$$\mathcal{H}(\theta) = \frac{1}{2} \|f(\phi^*, \theta)\|^2. \quad (65)$$

We use this formulation to provide an alternative proof to Theorem S1 that might be insightful for the reader.

Alternative proof of Theorem S1. Theorem S1 states that

$$\left(\frac{d}{d\theta} \mathcal{H}(\theta) \right)^\top = \frac{\partial f}{\partial \theta}(\phi^*, \theta)^\top f(\phi^*, \theta). \quad (66)$$

We use the shorthand notation $E := \frac{1}{2} \|f(\phi, \theta)\|^2$. The chain rule yields

$$\frac{d}{d\theta} E(\phi^*, \theta) = \frac{d}{d\theta} E(\phi^*, \theta) = \frac{\partial E}{\partial \theta}(\phi^*, \theta) + \frac{\partial E}{\partial \phi}(\phi^*, \theta) \frac{d\phi^*}{d\theta}. \quad (67)$$

As $\nabla_\phi L$ is independent of θ , we have that $d_\theta h(\phi^*) = 0$. This rewrites $\partial_\phi h(\phi^*) d_\theta \phi^* = 0$. This can be combined to the KKT conditions to show that the indirect term is equal to 0: right multiplying the condition

$$0 = \frac{\partial E}{\partial \phi}(\phi^*, \theta) + \mu^{*\top} \frac{\partial^2 L}{\partial y} (h(\phi^*)) \frac{\partial h}{\partial \phi}(\phi^*) \quad (68)$$

by $d_\theta \phi^*$ gives

$$\begin{aligned} 0 &= \frac{\partial E}{\partial \phi}(\phi^*, \theta) \frac{d\phi^*}{d\theta} + \mu^{*\top} \frac{\partial^2 L}{\partial y} (h(\phi^*)) \frac{\partial h}{\partial \phi}(\phi^*) \frac{d\phi^*}{d\theta} \\ &= \frac{\partial E}{\partial \phi}(\phi^*, \theta) \frac{d\phi^*}{d\theta}. \end{aligned} \quad (69)$$

This finishes the proof. \square

S2.6 The parameter update is robust to approximate optimal control

The purpose of this section is to formally prove that the first-order update prescribed by Theorem 1 is robust to inaccurate approximations of the optimally-controlled state ϕ^* . More precisely, we show that the quality of the gradient can be linked to the distance between the approximate and the true optimally-controlled state (Proposition S8) and that the update is minimizing a closely related objective when the perfect control limit is not exactly reached (Proposition S9).

Proposition S8. *Let ϕ_* be an optimally-controlled state and $\hat{\phi}$ an approximation of it that is used to update the parameters θ . Then, if the conditions of Theorem S1 apply and $\partial_\theta f(\phi, \theta)^\top f(\phi, \theta)$ is M -Lipschitz continuous we have that*

$$\left\| f(\hat{\phi}, \theta)^\top \frac{\partial f}{\partial \theta}(\hat{\phi}, \theta) - \frac{d}{d\theta} \mathcal{H}(\theta) \right\| \leq M \|\hat{\phi} - \phi_*\|. \quad (70)$$

Proof. We use Theorem S1 and then the Lipschitz continuity assumption:

$$\begin{aligned} \left\| f(\hat{\phi}, \theta)^\top \frac{\partial f}{\partial \theta}(\hat{\phi}, \theta) - \frac{d}{d\theta} \mathcal{H}(\theta) \right\| &= \left\| f(\hat{\phi}, \theta)^\top \frac{\partial f}{\partial \theta}(\hat{\phi}, \theta) - f(\phi^*, \theta)^\top \frac{\partial f}{\partial \theta}(\phi^*, \theta) \right\| \\ &\leq M \|\hat{\phi} - \phi^*\|. \end{aligned} \quad (71)$$

□

Proposition S9. *Let (ϕ_*, u_*) verifying the steady-state equations*

$$f(\phi_*, \theta) + Q(\phi_*, \theta)u_* = 0, \quad \text{and} \quad -\alpha u_* - \nabla_y L(h(\phi_*)) = 0. \quad (72)$$

If

$$Q(\phi_*, \beta) = \partial_\phi f(\phi_*, \theta)^{-\top} \partial_\phi h(\phi_*)^\top, \quad (73)$$

then ϕ_ is a stationary point of the augmented energy $F(\phi, \theta, \alpha) = \frac{1}{2} \|f(\phi, \theta)\|^2 + \alpha^{-1} L(h(\phi))$.*

Proof. We first use the formula for Q and use the steady-state equation on u_* :

$$\begin{aligned} 0 &= f(\phi_*, \theta) + Q(\phi_*, \theta)u_* \\ &= f(\phi_*, \theta) - \partial_\phi f(\phi_*, \theta)^{-\top} \partial_\phi h(\phi_*)^\top u_* \\ &= f(\phi_*, \theta) + \alpha^{-1} \partial_\phi f(\phi_*, \theta)^{-\top} \partial_\phi h(\phi_*)^\top \nabla_y L(h(\phi_*)) \end{aligned} \quad (74)$$

Left-multiplying by $\partial_\phi f(\phi_*, \theta)$ yields

$$\partial_\phi f(\phi_*, \theta)^\top f(\phi_*, \theta) + \alpha^{-1} \partial_\phi h(\phi_*)^\top \nabla_y L(h(\phi_*)) = 0, \quad (75)$$

which is exactly $\nabla_\phi F(\phi, \theta, \alpha) = 0$. □

Proposition S9 allows understanding what the update $\partial_\theta f(\phi_*, \theta)^\top f(\phi_*, \theta)$ is doing when the controlled dynamics reach an equilibrium, but α is non zero. In this case, we cannot guarantee that $Q(\phi_*, \theta)u_*$ is an optimal control. Still, when the strict condition on Q of Eq. 73 is satisfied (it is strict compared to the more general condition (35) of Theorem S2), the update prescribed by the least-control principle is minimizing $F(\phi_*, \theta, \alpha)$ as

$$\begin{aligned} \frac{d}{d\theta} F(\phi_*, \theta, \alpha) &= \frac{\partial F}{\partial \theta}(\phi_*, \theta, \alpha) + \frac{\partial F}{\partial \phi}(\phi_*, \theta, \alpha) \frac{d\phi_*}{d\theta} \\ &= \frac{\partial F}{\partial \theta}(\phi_*, \theta, \alpha) + 0 \\ &= \frac{\partial f}{\partial \theta}(\phi_*, \theta)^\top f(\phi_*, \theta). \end{aligned} \quad (76)$$

We showed in Section S2.5 that this objective is closely related to the least-control objective, and gets closer when $\alpha \rightarrow 0_+$. Note that the same conclusions apply if we use a proportional controller with strength β , at it verifies the steady-state equation (72) for $\alpha = \beta^{-1}$.

S2.7 Quick review of constrained optimization

We heavily rely on the Karush–Kuhn–Tucker (KKT) conditions and Lagrange multiplier method for characterizing constrained optimum. We state here some important properties that are throughout the proofs, and we refer the interested reader to [91, 92] for a comprehensive overview of the relevant theory.

KKT conditions. Consider the following equality-constrained optimization problem

$$\min_x f(x) \text{ s.t. } g(x) = 0, \quad (77)$$

with f some scalar function to be optimized and g a vector-valued function defining equality constraints on the set of feasible states. The corresponding Lagrangian is defined as

$$\mathcal{L}(x, \lambda) := f(x) + \lambda^\top g(x), \quad (78)$$

with λ the so-called Lagrange multipliers. It can be shown, e.g. Nocedal and Wright [91, Theorem 12.1], that local solutions x^* of the constrained optimization problem defined above satisfy the KKT conditions: there exists a Lagrange multiplier λ^* such that

$$\begin{cases} 0 = \frac{\partial f}{\partial x}(x^*) + \frac{\partial g}{\partial x}(x^*)\lambda^* \\ 0 = g(x) \end{cases} \quad (79)$$

or equivalently such that (x^*, λ^*) is a stationary point of the Lagrangian, i.e. $\partial_{x^*, \lambda^*} \mathcal{L}(x^*, \lambda^*) = 0$.

The KKT conditions are first-order stationary conditions for constrained optimization, in the same way $\partial_x f = 0$ is a stationary condition for unconstrained minimization. On the other side, there exists sufficient conditions under which those stationary conditions give a local, constrained or unconstrained, minimum. For unconstrained optimization, it can be that the Hessian $\nabla_x^2 f$ is positive definite. For constrained optimization there are several variants, but those conditions can more or less be understood as the Hessian $\partial_x^2 \mathcal{L}(x^*, \lambda^*)$ of the Lagrangian w.r.t. x is positive definite (see e.g. Nocedal and Wright [91, Theorem 12.5]).

Differentiating through minima. We now consider that both the objective f and the constraints g are dependent on some parameter y , and aim to calculate how $f(x^*(y), y)$ will react to a change in y , that is we aim to compute the gradient associated to

$$\min_y f(x^*(y), y) = \min_y \min_x f(x, y) \text{ s.t. } g(x, y) = 0. \quad (80)$$

For *unconstrained* bilevel optimization (i.e. without the equality constraints $g(x, y) = 0$), we differentiate through the inner minima $x^*(y)$ using the necessary stationary condition $\partial_x f(x^*(y), y) = 0$, combined with the implicit function theorem [87] to ensure that the implicit function $x^*(y)$ is well defined. This gives

$$\begin{aligned} \frac{d}{dy} f(x^*(y), y) &= \frac{\partial f}{\partial y}(x^*(y), y) + \frac{\partial f}{\partial x}(x^*(y), y) \frac{dx^*(y)}{dy} \\ &= \frac{\partial f}{\partial y}(x^*(y), y) + 0. \end{aligned} \quad (81)$$

Note that $d_y x^*(y)$ can be obtained via the implicit function theorem by using the first-order condition $\partial_x f(x^*(y), y) = 0$ but we do not need to compute it.

A similar technique can be applied to differentiate through a *constrained* minima. We first remark that x^* satisfies the KKT conditions so there exists a Lagrange multiplier $\lambda^*(y)$ such that

$$f(x^*(y), y) = \mathcal{L}(x^*(y), \lambda^*(y), y). \quad (82)$$

We then use the implicit function theorem on the KKT condition $\partial_{x, \lambda} \mathcal{L}(x^*, \lambda^*, y) = 0$ to show that the functions $x^*(y)$ and $\lambda^*(y)$ are well defined and differentiable, under the assumption that the Hessian of the Lagrangian w.r.t. x and λ is invertible. Finally, we have:

$$\begin{aligned} \frac{d}{dy} f(x^*(y), y) &= \frac{d}{dy} \mathcal{L}(x^*(y), \lambda^*(y), y) \\ &= \frac{\partial \mathcal{L}}{\partial y} + \frac{\partial \mathcal{L}}{\partial x} \frac{dx^*}{dy} + \frac{\partial \mathcal{L}}{\partial \lambda} \frac{d\lambda^*}{dy} \\ &= \frac{\partial \mathcal{L}}{\partial y} + 0 + 0 \end{aligned} \quad (83)$$

where the last inequality holds as $x^*(y)$ and $\lambda^*(y)$ are stationary points of the Lagrangian \mathcal{L} .

S3 Implicit gradient, recurrent backpropagation and the link to the least-control principle

The least-control principle aims at solving the learning problem

$$\min_{\theta} L(h(\phi^*)) \quad \text{s.t.} \quad f(\phi^*, \theta) = 0 \quad (84)$$

indirectly, by minimizing the least-control objective. This leads to first-order updates, contrary to the direct minimization of the loss $L(\phi^*)$. In this section, we derive the implicit gradient associated to direct loss minimization, show how the recurrent backpropagation computes it, and finally highlight the similarities behind the least control principle and recurrent backpropagation.

Implicit gradient. The implicit gradient $d_{\theta}L(\phi^*)$ can be calculated analytically using the implicit function theorem [87], we here calculate it. The quantity ϕ^* can be characterized as an implicit function of θ , which verifies

$$f(\phi^*, \theta) = 0 \quad (85)$$

for all θ . The implicit function theorem guarantees that ϕ^* is properly defined as an implicit function of θ if $\partial_{\phi}f(\phi^*, \theta)$ is invertible, and then

$$\frac{d\phi^*}{d\theta} = - \left(\frac{\partial f}{\partial \phi}(\phi^*, \theta) \right)^{-1} \frac{\partial f}{\partial \theta}(\phi^*, \theta).$$

We can then use the chain rule to obtain the implicit gradient:

$$\begin{aligned} \frac{d}{d\theta} L(h(\phi^*)) &= \frac{\partial L}{\partial y}(h(\phi^*)) \frac{\partial h}{\partial \phi}(\phi^*) \frac{d\phi^*}{d\theta} \\ &= - \frac{\partial L}{\partial y}(\phi^*) \frac{\partial h}{\partial \phi}(h(\phi^*)) \left(\frac{\partial f}{\partial \phi}(\phi^*, \theta) \right)^{-1} \frac{\partial f}{\partial \theta}(\phi^*, \theta). \end{aligned} \quad (86)$$

Recurrent backpropagation. The implicit gradient is computationally intractable for most of practical applications due to the matrix inversion. The key idea behind the recurrent backpropagation algorithm is that the column vector

$$\pi^* := \left(\frac{\partial f}{\partial \phi}(\phi^*, \theta) \right)^{-\top} \frac{\partial h}{\partial \phi}(\phi^*)^{\top} \frac{\partial L}{\partial y}(h(\phi^*))^{\top} \quad (87)$$

is the steady state of the dynamics

$$\dot{\pi} = \left(\frac{\partial f}{\partial \phi}(\phi^*, \theta) \right)^{\top} \pi - \frac{\partial h}{\partial \phi}(\phi^*)^{\top} \frac{\partial L}{\partial y}(h(\phi^*))^{\top} \quad (88)$$

or alternatively the fixed point of the iterative procedure

$$\pi_{\text{next}} = \pi + \left(\frac{\partial f}{\partial \phi}(\phi^*, \theta) \right)^{\top} \pi - \frac{\partial h}{\partial \phi}(\phi^*)^{\top} \frac{\partial L}{\partial y}(h(\phi^*))^{\top}. \quad (89)$$

Once π^* , or its estimation, is obtained through this dynamical procedure, it can then be used to estimate the implicit gradient with

$$\frac{d}{d\theta} L(\phi^*) = -\pi^{*\top} \frac{\partial f}{\partial \theta}(\phi^*, \theta) \quad (90)$$

Comparison with the least-control principle. We now compare the implicit gradient, as computed with recurrent backpropagation, with the gradient of the least-control objective, which is equal to

$$\frac{d\mathcal{H}}{d\theta}(\theta) = -\psi^{*\top} \frac{\partial f}{\partial \theta}(\phi^*, \theta) \quad (91)$$

as given by Theorem 1. In addition to the close resemblance between the gradients (90) and (91), the dynamical equations on π and ψ share some interesting similarities. Let us take the example of the inversion dynamics

$$\begin{aligned} \dot{\phi} &= f(\phi, \theta) + \psi \\ \dot{\psi} &= \left(\frac{\partial f}{\partial \phi}(\phi, \theta) \right)^{\top} \psi + \frac{\partial h}{\partial \phi}(\phi)^{\top} u \end{aligned} \quad (92)$$

of Eq. 8. The ψ dynamics are very similar to the one of π : they can be understood as multiplying the inverse of the Jacobian of f with an error minimization signal, that is either $-\partial_y L$ or u , to yield π^* or ψ^* . The important conceptual difference is that the controlled dynamics of the least-control principle simultaneously compute both the steady state ϕ_* and optimal control ψ_* in a single phase, whereas recurrent backpropagation uses two separate phases for computing ϕ^* and π^* . This unique feature of the least-control principle is made possible by letting the control ψ influence the dynamics and hence the steady state of ϕ .

S4 On the relation between the least-control principle, free energy and predictive coding

Predictive coding [35, 36, 55, 57, 93] emerged as an important framework to study perception and sensory processing in the brain. In this framework, the brain is assumed to maintain a probabilistic model of the environment, which is constantly used to perform inference on its sensory inputs. Here, we expand in more detail on the relation between our least-control principle and predictive coding. More specifically, we discuss how the constrained energy minimization of Eq. 9 relates to the free energy used in recent work on supervised predictive coding [35], and how the new insights of the least-control principle, such as more flexible dynamics, translate to the predictive coding framework.

S4.1 Supervised predictive coding

The starting point of standard predictive coding theories is the specification of a probabilistic generative model from latent causes towards sensory inputs; this model is then used to infer the most likely causes underlying incoming sensory stimuli. Recent work [35] investigated supervised predictive coding, a form of predictive coding where the direction of causality is flipped, i.e., where one uses a discriminative model from sensory inputs towards latent causes, and trains this model by clamping its outputs to the correct teacher value and performs inference to propagate teaching signals throughout the network. Whittington and Bogacz [35] related the parameter updates resulting from supervised predictive coding network to error backpropagation [33, 34] when the output is weakly nudged towards the teacher value instead of being clamped. In Section S4.3 we show that the least-control principle relates the supervised predictive coding updates with standard teacher clamping to gradient updates on the least-control objective (3) thereby removing the need for the weak-nudging limit.

Supervised predictive coding uses a probabilistic latent variable model to compute the likelihood $p(y | x; \theta)$ of the output y given the sensory input x . More specifically, it uses a hierarchical Gaussian model, a particular type of directed acyclic graphical model, with the following factorized distribution

$$\begin{aligned}
 p(z_1, \dots, z_{L-1}, y | x; \theta) &= p(y | z_{L-1}) \prod_{l=1}^{L-1} p(\phi_l | z_{l-1}) \\
 p(z_l | \phi_{l-1}) &= \mathcal{N}(z_l; W_l \sigma(z_{l-1}), \Sigma_l) \\
 p(y | z_{L-1}) &= \mathcal{N}(y; W_L \sigma(z_{L-1}), \Sigma_y)
 \end{aligned} \tag{93}$$

with latent variables $z = \{z_l\}_{l=1}^{L-1}$, parameters $\theta = \{W_l\}_{l=1}^L, \mathcal{N}(v; \mu, \Sigma)$ a Gaussian distribution over a variable v with mean μ and correlation matrix Σ , and where we take $\sigma(z_0) = x$. The goal of training this model is to change the model parameters W_l to maximize the marginal likelihood for input-output pairs (x, y) :

$$p(y | x; \theta) = \int p(z, y | x; \theta) dz \tag{94}$$

As optimizing this marginal directly is intractable, predictive coding uses the variational expectation maximization method [93–96]. This method uses a variational distribution $q(z; \phi)$ with parameters ϕ to approximate the posterior $p(z | x, y)$ and then defines the free energy \mathcal{F} as an upper bound on the negative log-likelihood:

$$\begin{aligned}
 \mathcal{F}(\phi, \theta) &= -\mathbb{E}_q[\log p(y, z | x; \theta)] + \mathbb{E}_q[\log q(z; \phi)] \\
 &= -\log p(y | x; \theta) + D_{\text{KL}}(q(z; \phi) || p(z | x, y; \theta)) \geq -\log p(y | x; \theta),
 \end{aligned} \tag{95}$$

with D_{KL} the KL divergence which is always positive. Now the variational expectation maximization method proceeds in two alternating phases. In the expectation phase, it minimizes the free energy \mathcal{F} w.r.t. ϕ for the current parameter setting of θ , i.e. it finds a good approximation $q(z; \phi)$ for the posterior. In the maximization phase, it minimizes the free energy w.r.t. θ for the updated parameter setting of ϕ .

To be able to perform the two phases using simple neural dynamics and local update rules, predictive coding uses the Dirac delta distribution $q(z; \phi) = \delta(z - \phi)$ as the variational distribution [96]. Now, the entropy term $\mathbb{E}_q[\log p(y, z | x; \theta)]$ is independent of ϕ and hence we ignore it in the expectation

and maximization step.² Taken together, this result in the following free energy (without entropy term):

$$\begin{aligned}\mathcal{F}(\phi, \theta) &= -\log p(y, \phi | x; \theta) \\ &= \rho \frac{1}{2} \|y - W\sigma(\phi_{L-1})\|^2 + \frac{1}{2} \sum_{l=1}^{L-1} \|\phi_l - W_l \sigma(\phi_{l-1})\|^2 + C\end{aligned}\quad (96)$$

with C a constant independent of ϕ and θ , $x = \sigma(\phi_0)$, and where we took for simplicity $\Sigma_l = \text{Id}$ and $\Sigma_y = \rho^{-1} \text{Id}$. For the expectation step, predictive coding interprets the parameters $\phi = \{\phi_l\}_{l=1}^{L-1}$ as a prediction neuron population and uses the gradient flow on \mathcal{F} w.r.t. ϕ as neural dynamics to find a ϕ_* that minimizes \mathcal{F} . For the maximization step, predictive coding performs a gradient step on $\mathcal{F}(\phi_*, \theta)$ w.r.t. θ , evaluated at the steady-state neural activity ϕ_* . Thus,

$$\begin{aligned}\dot{\phi} &= -\frac{\partial \mathcal{F}}{\partial \phi}(\phi, \theta)^\top, \\ \Delta\theta &= -\frac{\partial \mathcal{F}}{\partial \theta}(\phi_*, \theta)^\top,\end{aligned}\quad (97)$$

with the change $\Delta\theta$ applied after the neural dynamics has converged, i.e., when $\dot{\phi} = 0$.

S4.2 Equivalence between the free and augmented energies

To link supervised predictive coding to the least-control principle, we further manipulate the free energy of Eq. 96 to relate it to the augmented energy $F = \frac{1}{2} \|f(\phi, \theta)\|^2 + \beta L$ introduced in Section 2.4. For this, we introduce a ‘ghost layer’ z_L in between z_{L-1} and y , that exists solely for the purpose of analyzing the free energy. The joint probability distribution is now given by

$$\begin{aligned}p(z, y | x; \theta) &= p(y | z_L) \prod_{l=1}^L p(z_l | z_{l-1}) \\ p(z_l | z_{l-1}) &= \mathcal{N}(z_l; W_l \sigma(z_{l-1}), \text{Id}) \\ p(y | z_L) &= \mathcal{N}(y; z_L, \beta^{-1} \text{Id})\end{aligned}\quad (98)$$

We recover the same marginal likelihood $p(y | x; \theta)$ as before if we have that $\rho^{-1} = \beta^{-1} + 1$, assuming that $\rho^{-1} > 1$. Using again the dirac delta distribution as variational distribution, we get the following augmented free energy

$$\begin{aligned}\mathcal{F}(\phi, \theta, \beta) &= \log p(\phi, y | x; \theta) = \frac{1}{2} \sum_{l=1}^L \|\phi_l - W_l \sigma(\phi_{l-1})\|^2 + \beta \frac{1}{2} \|y - \phi_L\|^2 \\ &= \frac{1}{2} \|\phi - W\sigma(\phi) - Ux\|^2 + \beta L(D\phi)\end{aligned}\quad (99)$$

$$W = \begin{bmatrix} 0 & 0 & 0 & 0 \\ W_2 & 0 & 0 & 0 \\ 0 & \ddots & 0 & 0 \\ 0 & 0 & W_L & 0 \end{bmatrix}, \quad U = \begin{bmatrix} W_1 \\ 0 \end{bmatrix}, \quad D = [0 \quad \text{Id}],$$

with ϕ the concatenation of $\{\phi_l\}_{l=1}^L$, L the squared error loss and where we ignored the constant term C . Hence, we see that the free energy used in predictive coding is equivalent to the augmented energy $F = \frac{1}{2} \|f(\phi, \theta)\|^2 + \beta L$ introduced in Section 2.4. Consequently, we can use the least-control principle to characterize predictive coding in the limit of $\beta \rightarrow \infty$.

²Note however that this entropy term is infinite for the delta distribution, hence for making the derivation rigorous, certain limits need to be taken. For example, Friston et al. [93] uses a Laplace approximation instead of the delta distribution.

S4.3 Learning with teacher clamping results in gradients on the least-control objective

Whittington and Bogacz [35] connected supervised predictive coding to gradient-based optimization of the loss L , when the variance of the output layer y goes to infinity. In this limit, there is only an infinitesimal effect of the teaching signal on the rest of the network, arising by clamping y towards y^{true} , as the model ‘does not trust’ the output layer y by construction. This *weak nudging* limit is captured in the augmented energy of Eq. (99) as the limit of $\beta \rightarrow 0$, and can be linked to gradient-based optimization of the loss L for more general energy functions beyond predictive coding [24].

Equipped with the least-control principle, we can now relate predictive coding to gradient-based optimization on the least-control objective of Eq. 3, without the need for infinite variance in the output layer. In Sections 2.4 and S2.5, we show that when the neural dynamics minimize the augmented energy $F(\phi, \theta, \beta)$ for $\beta \rightarrow \infty$, the parameter update $\Delta\theta$ of Eq. 97 follows the gradient on the least-control objective (3). This perfect control limit of $\beta \rightarrow \infty$ corresponds to the conventional teacher clamping setting, where the output y has a finite variance (without loss of generality, $\rho = 1$ in this case in our derivation, as $\rho^{-1} = \beta^{-1} + 1$).

S4.4 The optimal control interpretation of predictive coding leads to flexible dynamics.

Now that we connected predictive coding to the least-control principle, we can further investigate predictive coding through the lens of optimal control. In predictive coding, the neural dynamics follow the gradient flow on the augmented free energy \mathcal{F} of Eq. (99):

$$\begin{aligned} \dot{\phi} &= -\frac{\partial \mathcal{F}}{\partial \phi}(\phi, \theta, \beta)^\top \\ &= -\phi + W\sigma(\phi) + Ux + \sigma'(\phi)W^\top(\phi - W\sigma(\phi) - Ux) - \beta D^\top \nabla_y L(D\phi) \end{aligned} \quad (100)$$

with $\sigma'(\phi) = \partial_\phi \sigma(\phi)$. For $\beta \rightarrow \infty$, the last term $\beta D^\top \nabla_y L(D\phi)$ corresponds to an infinitely fast proportional control that clamps the output $y = \phi_L$ to the teacher y^{true} . The term $\sigma'(\phi)W^\top(\phi - W\sigma(\phi) - Ux)$ then optimally propagates the control at the output level towards the rest of the network. In predictive coding, the term $\phi - W\sigma(\phi) - Ux$ is usually interpreted as an error neuron population ψ . Hence, in the optimal control view, the error neuron population ψ optimally controls the prediction neuron population ϕ to reach a controlled network state that exactly matches the output target y^{true} , while having the smallest possible error signals $\|\psi\|^2 = \|\phi - W\sigma(\phi) - Ux\|^2$. This view is further corroborated by isolating the error neurons ψ at the equilibrium of the neural dynamics (100), leading to $\psi_* = -(I - W\sigma'(\phi_*))^{-\top} D^\top \beta \nabla_y L(D\phi_*)$, which satisfies the column space condition of Theorem 2 with $u_* = -\beta \nabla_y L(D\phi_*)$, confirming that the error neurons steady state ψ_* is an optimal control.

Importantly, using the least-control principle, we can go beyond the gradient-flow dynamics on F and generalize the predictive coding framework to more flexible neural dynamics. First, instead of clamping the output of the network towards the teacher value with an infinitely fast proportional controller, one can use more general output controllers that satisfy the equilibrium condition $\alpha u_* + \nabla_y L(D\phi) = 0$ for $\alpha \rightarrow 0$, such as an integral controller. Next, as we identified the error neurons $\psi = \phi - W\sigma(\phi) - Ux$ as being an optimal control, we can use any dynamics satisfying Theorem 2 to compute these optimal error neurons ψ and resulting neural dynamics $\dot{\phi}$. For example, we can use the inversion dynamics of Eq. 8 and 14 to dynamically compute the error neuron activity ψ . Strikingly, at the steady state, the error neurons computed with these inversion dynamics are indistinguishable from the error neurons computed with the energy-based dynamics of Eq. 100, even though the underlying dynamics and hence circuit implementation are completely different. This ‘circuit invariance’ under the optimality condition of Theorem 2 opens new routes towards finding cortical circuits implementing predictive coding, which is a topic of high relevance in neuroscience [57]. Furthermore, the least-control principle allows unifying predictive coding with other existing theories for learning in the brain [17, 29] by uncovering possible equivalences of the underlying credit assignment techniques.

S4.5 Beyond feedforward neural networks.

The underlying theory of predictive coding, which starts from an acyclic graphical model, is tailored towards feedforward neural networks. However, starting from the augmented energy F of Eq. (99),

we can generalize predictive coding to equilibrium recurrent neural networks with arbitrary synaptic connectivity matrices W and U . Although the link with probabilistic latent variable models is not straightforwardly extendable to equilibrium RNNs, the predictive coding interpretation based on error and prediction neurons remains valid. To the best of our knowledge, our experiments testing this new setting of predictive coding for equilibrium RNNs are the first of their kind.

S5 Remarks on the least-control principle when using multiple data points

Without loss of generality, we consider a single data point in the formulation of the least-control principle in Section 2, for clarity of presentation. Here, we discuss in more detail how multiple data points can be incorporated in the least-control principle.

S5.1 Loss defined over finite sample of data points

In many learning problems, as in supervised learning, the loss L is defined over a finite set of data samples:

$$L(\phi) = \sum_{b=1}^B L^b(\phi). \quad (101)$$

As the losses associated to different samples are different, the corresponding teaching signal will impact the state differently. We therefore consider ϕ to be a concatenation of all the sample-specific states $\{\phi^b\}_{b=1}^B$. The loss is then equal to

$$L(\phi) = \sum_{b=1}^B L^b(\phi^b). \quad (102)$$

Similarly, we define $f(\phi, \theta)$ as a concatenation of all $f(\phi^b, \theta)$, and ψ as a concatenation of all the controls ψ^b . We can then apply the least-control principle on this concatenated quantities.

As the least-control objective of Eq. 3 can be rewritten as the sum $\sum_b \|\psi^{*b}\|^2$, and has constraints that do not interact in between different datapoints b , its gradient can also be rewritten as a sum over the datapoints:

$$\frac{d\mathcal{H}}{d\theta}(\theta) = \sum_{b=1}^B \frac{d\mathcal{H}^b}{d\theta}(\theta) \quad (103)$$

with $\mathcal{H}^b(\theta)$ the least-control objective for a single data point b . It follows that one can use standard stochastic or mini-batch optimization methods to minimize the least-control objective $\mathcal{H}(\theta)$.

S5.2 Loss defined by expectation over an infinite inputspace

When there exists an infinite number of data samples (e.g. a continuous input space), the loss can be defined as an expectation over this infinity of data samples:

$$L(\phi) = \mathbb{E}_b[L_b(\phi)] \quad (104)$$

One approach to incorporate this case in the least-control principle is to first sample a finite amount of data samples, and then apply the arguments of Section S5.1.

Another approach is to define the least-control objective as an expectation over the infinity of samples:

$$\begin{aligned} \mathcal{H}(\theta) &= \mathbb{E}_b[\mathcal{H}^b(\theta)] \\ \mathcal{H}^b(\theta) &= \min_{\phi^b, \psi^b} \|\phi^b\|^2 \quad \text{s.t. } f(\phi^b, \theta) + \psi^b = 0, \quad \nabla_y L(h(\phi^b)) = 0 \end{aligned} \quad (105)$$

Then, under standard regularity conditions for exchanging the gradient and expectation operator, we can sample gradients of this least-control objective:

$$\frac{d\mathcal{H}}{d\theta}(\theta) = \mathbb{E} \left[\frac{d\mathcal{H}^b}{d\theta}(\theta) \right] \quad (106)$$

with $d_\theta \mathcal{H}^b(\theta)$ given by Theorem 1.

S6 The least-control principle for equilibrium RNNs

Here, we provide additional details on the equilibrium recurrent neural network models, the derivation of the local learning rules and the various controller designs.

S6.1 Equilibrium recurrent neural network model specifications

We use an equilibrium RNN with the following free dynamics:

$$\dot{\phi} = f(\phi, \theta) = -\phi + W\sigma(\phi) + Ux, \quad (107)$$

with ϕ the neural activities of the recurrent layer, W the recurrent synaptic weight matrix, U the input weight matrix and σ the activation function. We evaluate the performance of this RNN at equilibrium, by selecting a set of output neurons and measuring its loss $L(D\phi^*)$, with $D = [0 \text{ Id}]$ a fixed decoder matrix.

Learning a decoder matrix. In practice, we can achieve better performance if we learn a decoder matrix to map the recurrent activity ϕ to the output y , instead of taking a fixed decoder $D = [0 \text{ Id}]$. To prevent the loss $L(D\phi)$ from depending on the learned parameters θ , we augment the recurrent layer ϕ with an extra set of output neurons, and include a learned decoder matrix \tilde{D} inside the augmented recurrent weight matrix \bar{W} , leading to the following free dynamics:

$$\begin{aligned} \dot{\bar{\phi}} &= f(\bar{\phi}, \theta) = -\bar{\phi} + \bar{W}\sigma(\bar{\phi}) + \bar{U}x, \\ \bar{W} &= \begin{bmatrix} W & 0 \\ \tilde{D} & 0 \end{bmatrix}, \quad \bar{U} = \begin{bmatrix} U \\ 0 \end{bmatrix}, \end{aligned} \quad (108)$$

with $\bar{\phi}$ the concatenation of ϕ with a set of output neurons and $\theta = \{W, U, \tilde{D}\}$ the set of learned parameters. To map the augmented recurrent layer $\bar{\phi}$ to the output y , we again use a fixed decoder $D = [0 \text{ Id}]$ that selects the ‘output neurons’ in $\bar{\phi}$. At equilibrium, we now have $y = D\bar{\phi} = \tilde{D}\sigma(\phi)$. Hence, we see that at equilibrium, the augmented system of Eq. 108 with a fixed decoder D and hence a loss $L(D\bar{\phi})$ independent of θ is equivalent to the original system of Eq. 107 with a learned decoder D and loss $L(D\sigma(\phi))$. We can now use the least-control principle on the augmented system of Eq. 108 to learn the weight matrices $\theta = \{W, U, \tilde{D}\}$, which we show in the next section.

Including biases. In practice, we equip the neurons with a bias parameter b , leading to the following free dynamics

$$\dot{\phi} = f(\phi, \theta) = -\phi + W\sigma(\phi) + Ux + b, \quad (109)$$

with the set of learned parameters $\theta = \{W, U, b\}$. This can be extended to the augmented system of Eq. 108 by adding the augmented bias parameters \bar{b} , which is a concatenation of the original bias b and the decoder bias \tilde{b} . At equilibrium, we now have $y = D\bar{\phi} = \tilde{D}\sigma(\phi) + \tilde{b}$. For ease of notation, we omit the bias terms in most of the derivations in this paper.

Link with feedforward neural networks. When the recurrent weight matrix has a lower block-diagonal structure, the equilibrium of the RNN corresponds to a conventional deep feedforward neural network. More specifically, taking

$$W = \begin{bmatrix} 0 & 0 & 0 & 0 \\ W_2 & 0 & 0 & 0 \\ 0 & \ddots & 0 & 0 \\ 0 & 0 & W_L & 0 \end{bmatrix}, \quad U = \begin{bmatrix} W_1 \\ 0 \end{bmatrix}, \quad D = [0 \text{ Id}], \quad (110)$$

gives the following feedforward mappings at equilibrium

$$\phi_l = W_l\sigma(\phi_{l-1}) + b_l, \quad 1 \leq l \leq L \quad (111)$$

where we structure ϕ into L layers ϕ_l , and take $\sigma(\phi_0) = x$ and $y = D\phi = \phi_L$. Hence, we see that the equilibrium RNN model also includes the conventional deep feedforward neural network.

Fixed point iterations. For computational efficiency, we use fixed point iterations for finding the equilibrium of the free dynamics (107), which we need for the recurrent backpropagation baseline, and for evaluating the test performance of the trained equilibrium RNN.

$$\phi_{\text{next}} = W\sigma(\phi) + Ux \quad (112)$$

S6.2 Deriving a local learning rule for equilibrium RNNs

The least-control principle prescribes to augment the RNN dynamics of Eq. 107 with an optimal controller ψ that leads the neural dynamics to a controlled equilibrium ϕ_* , where the output neurons $y_* = D\phi_*$ minimize the loss L , while being of minimum norm $\|\psi^*\|$. This optimal control contains a useful learning signal, which we leverage in Theorem 1 to derive local first-order parameter updates $\Delta\theta = -d_\theta \mathcal{H}(\theta) = \psi^{*\top} \partial_\theta f(\phi^*, \theta)$, with (ψ^*, ϕ^*) the minimizers of the least-control problem of Eq. 3, i.e. the optimal control and optimally controlled state, respectively. In the next sections, we discuss in detail how to compute (ψ^*, ϕ^*) for the equilibrium RNN using neural dynamics. Here, we apply the first-order update $\Delta\theta$ to the equilibrium RNN to arrive at the local synaptic updates of Eq. 12.

Derivation of the local update rules. To avoid using tensors in $\partial_\theta f(\phi^*, \theta)$, we vectorize the weight matrices W and U and use Kronecker products to rewrite the free dynamics of Eq. 107:³

$$\dot{\phi} = -\phi + (\sigma(\phi)^\top \otimes \text{Id})\vec{W} + (x^\top \otimes \text{Id})\vec{U} + b \quad (113)$$

with \otimes the Kronecker product, Id the identity matrix and \vec{W} and \vec{U} the vectorized form (concatenated columns) of W and U , respectively. Taking θ the concatenation of \vec{W} , \vec{U} and b , we get

$$\Delta\theta = \psi^{*\top} \frac{\partial f}{\partial \theta}(\phi^*, \theta) = \psi^{*\top} [(\sigma(\phi)^\top \otimes \text{Id}) \quad (x^\top \otimes \text{Id}) \quad \text{Id}] \quad (114)$$

We can rewrite the resulting update in matrix form again, leading to the following parameter updates for the RNN:

$$\Delta W = \psi^* \sigma(\phi^*)^\top, \quad \Delta U = \psi^* x^\top, \quad \Delta b = \psi^*. \quad (115)$$

Now assuming we have a controller ψ that leads the dynamics to the optimally controlled state $(\psi_*, \phi_*) = (\psi^*, \phi^*)$, we arrive at the updates of Eq. 12. Note that we can use these updates in any gradient-based optimizer. Applying a similar derivation to the augmented RNN dynamics of Eq. 108, we arrive at the following updates for $\theta = \{W, U, b, \tilde{D}, \tilde{b}\}$:

$$\Delta W = \psi^* \sigma(\phi^*)^\top, \quad \Delta U = \psi^* x^\top, \quad \Delta \tilde{D} = \tilde{\psi}^* \sigma(\phi^*)^\top, \quad \Delta b = \psi^*, \quad \Delta \tilde{b} = \tilde{\psi}^* \quad (116)$$

with $\tilde{\psi}$ the control applied on the set of output neurons within $\bar{\phi}$, and ψ the control applied to the set of recurrent neurons ϕ (i.e. $\bar{\phi}$ without the output neurons).

Controller dynamics. Theorem 2 shows that we can compute an optimal control ψ^* by using any controller ψ that leads the system to a controlled equilibrium

$$0 = f(\phi_*, \theta) + Q(\phi_*, \theta)u_*, \quad 0 = -\alpha u_* - \frac{\partial L}{\partial y}(h(\phi_*))^\top \quad (117)$$

in the limit of $\alpha \rightarrow 0$ and with $Q(\phi_*, \theta)$ satisfying the column space condition

$$\text{col}[Q(\phi_*, \theta)] = \text{row} \left[\frac{\partial h}{\partial \phi}(\phi_*) \left(\frac{\partial f}{\partial \phi}(\phi_*, \theta) \right)^{-1} \right]. \quad (118)$$

Under these conditions, we have that $Q(\phi_*, \theta)u_*$ is an optimal control ψ^* . Applied to the equilibrium RNN setting, this result in the following column space condition.

$$\text{col}[Q(\phi_*, \theta)] = \text{row} \left[D(\text{Id} - W\sigma'(\phi_*))^{-1} \right], \quad (119)$$

with $\sigma'(\phi) := \partial_\phi \sigma(\phi)$. In the next sections, we propose various control dynamics $\dot{\psi}$ that satisfy these conditions at equilibrium and hence lead to an optimal control ψ^* .

S6.3 A controller with direct linear feedback

We start with the simplest controller, that broadcasts the output controller u to the recurrent neurons ϕ with a direct linear mapping Q , resulting in the following dynamics:

$$\tau \dot{\phi} = -\phi + W\sigma(\phi) + Ux + Qu, \quad \tau_u \dot{u} = -\frac{\partial L}{\partial y}(D\phi)^\top - \alpha u, \quad (120)$$

with τ and τ_u the time constants of the neural dynamics and output controller dynamics, respectively. We assume without further discussion that the output controller u which integrates the output error $\partial_y L$ is implemented by some neural integrator circuit, a topic which has been extensively studied elsewhere [97].

³For this, we use the following property: $\text{vec}(ABC) = (C^\top \otimes A)\text{vec}(B)$, with vec the vectorization operator that concatenates the columns of a matrix and \otimes the Kronecker product.

S6.3.1 A single-phase learning scheme for updating the feedback weights

Theorem 2 guarantees that this dynamics converges to the optimal control ψ^* if the column space condition of Eq. 119 is satisfied. As Q is now a linear mapping, this condition cannot be exactly satisfied for all samples in the dataset, as the right-hand side of Eq. 119 is data-dependent, whereas Q is not. Still, we learn the feedback weights Q simultaneously with the other weights W and U , to approximately fulfill this column space condition, without requiring separate phases. For this, we add noise to the dynamics and we adapt a recently proposed feedback learning rule for feedforward neural networks [29, 50] towards our RNN setup, leading to the following system dynamics and simple anti-Hebbian plasticity dynamics:

$$\tau \dot{\phi} = -\phi + W\sigma(\phi) + Ux + Qu + s\epsilon \quad (121)$$

$$\tau_Q \dot{Q} = -s\epsilon u_{\text{hp}}^\top - \gamma_Q Q \quad (122)$$

Here, γ_Q is a small weight-decay term, ϵ is noise from an Ornstein-Uhlenbeck process, i.e. exponentially filtered white noise with standard deviation s and timeconstant τ_ϵ . As post-synaptic plasticity signal, we use a high-pass filtered version u_{hp} of the output control u , to extract the noise fluctuations. We model the plasticity with continuous dynamics instead of a single update at equilibrium, as the noise ϵ changes continuously. Building upon the work of Meulemans et al. [29, 50], we show in Proposition S10 that the feedback learning dynamics of Eq. 122 drives the feedback weights to a setting that satisfies the column space condition of Eq. 119, when trained on a single data point.

Proposition S10. *Assuming (i) a separation of timescales $\tau \ll \tau_\epsilon \ll \tau_u \ll \tau_Q$, (ii) a small noise variance $s^2 \ll \|\phi\|^2$, (iii) a high-pass filtered control signal $u_{\text{hp}} = u - u_{\text{ss}}$ with u_{ss} the steady state of the first moment of the output controller trajectory u , and (iv) stable dynamics, then, for a single fixed input x , the feedback learning dynamics of Eq. 122 let the first moment $\mathbb{E}[Q]$ converge towards a setting satisfying the column space condition of Theorem 2:*

$$\mathbb{E}[Q_{\text{ss}}^\top] \propto \frac{\partial^2 L}{\partial y^2} (D\phi_{\text{ss}}) D(\text{Id} - W\sigma'(\phi_{\text{ss}}))^{-1} \quad (123)$$

with ϕ_{ss} the steady state of the first moment of the state trajectory ϕ , and $\sigma'(\phi) = \partial_\phi \sigma(\phi)$.

Proof. The general idea behind the feedback learning rule of Eq. 122 is to correlate the noise fluctuations of the output controller u with the noise ϵ inside the neurons that caused these fluctuations. As the injected noise propagates through the whole network, and the neural dynamics $\dot{\phi}$ evolve on a faster timescale compared to the noise ϵ , the noise fluctuations in the output contain useful information on the network transformation $D(\text{Id} - W\sigma')^{-1}$ which can be extracted by correlating these fluctuations with the noise ϵ . We refer the interested reader to Appendix C of Meulemans et al. [29] for a detailed discussion of this type of feedback learning rule for feedforward neural networks.

First, we define the neural fluctuations $\tilde{\phi} := \phi - \phi_{\text{ss}}$ and output controller fluctuations $\tilde{u} = u - u_{\text{ss}}$, with ϕ_{ss} and u the steady state of the first moment of ϕ and u , respectively. Using the assumption that the noise variance s^2 is much smaller than the neural activity $\|\phi\|^2$ and that we have stable (hence contracting) dynamics, we perform a first-order Taylor approximation around ϕ_{ss} and u , which for simplicity we assume to be exact, leading to the following dynamics:

$$\tau \dot{\tilde{\phi}} = -\tilde{\phi} + W\sigma'(\phi_{\text{ss}})\tilde{\phi} + Q\tilde{u} + \epsilon, \quad (124)$$

$$\tau_u \dot{\tilde{u}} = \frac{\partial^2 L}{\partial y^2} (D\phi_{\text{ss}}) D\tilde{\phi} - \alpha\tilde{u} \quad (125)$$

where we used that $-\phi_{\text{ss}} + W\sigma(\phi_{\text{ss}}) + Ux + Qu_{\text{ss}} = 0$ and $-\partial_y L(D\phi_{\text{ss}}) - \alpha u_{\text{ss}} = 0$ by definition. To compress notation, we introduce the variable ν as a concatenation of $\tilde{\phi}$ and \tilde{u} .

$$\begin{aligned} \dot{\nu} &= -A\nu + B\epsilon \\ A &:= \begin{bmatrix} \frac{1}{\tau}(\text{Id} - W\sigma'(\phi_{\text{ss}})) & -\frac{1}{\tau}Q \\ \frac{1}{\tau_u}\frac{\partial^2 L}{\partial y^2}(D\phi_{\text{ss}})D & \frac{\alpha}{\tau_u}\text{Id} \end{bmatrix} & B &:= \begin{bmatrix} \frac{s}{\tau}\text{Id} \\ 0 \end{bmatrix} \end{aligned} \quad (126)$$

We solve this linear time-invariant stochastic differential equation using the method of variation of constants [98], while assuming that $\nu = 0$ at time t_0 , i.e. that the dynamics already have converged to the steady state at t_0 .

$$\nu(t) = \int_{t_0}^t \exp(-A(t-t')) B\epsilon(t') dt'. \quad (127)$$

Now we turn to the first moment of the feedback weight learning (122), using $\tilde{u} = C\nu$ with $C = [0 \text{ Id}]$:

$$\mathbb{E} [\tilde{u}(t)\epsilon(t)^\top] = C\mathbb{E} [\nu(t)\epsilon(t)^\top] = \frac{1}{2\tau_\epsilon} C \int_{t_0}^t \exp\left(-\left(A + \frac{1}{\tau_\epsilon} \text{Id}\right)(t-t')\right) B dt' \quad (128)$$

for which we used that $\mathbb{E} [\epsilon(t)\epsilon(t')^\top] = \frac{1}{2\tau_\epsilon} \exp(-\frac{1}{\tau_\epsilon}|t-t'|)$ for an Ornstein-Uhlenbeck process with timeconstant τ_ϵ . Now assuming that $t \gg t_0$ and that we have stable dynamics (i.e. A has strictly positive eigenvalues), we can solve the integral of the matrix exponential:

$$\mathbb{E} [\tilde{u}(t)\epsilon(t)^\top] = \frac{1}{2\tau_\epsilon} C \left(A + \frac{1}{\tau_\epsilon} \text{Id}\right)^{-1} B \quad (129)$$

We solve the inverse of this 2×2 block matrix analytically (following e.g. Lu and Shiou [99]), leading to

$$\begin{aligned} \mathbb{E} [\tilde{u}(t)\epsilon(t)^\top] &= \frac{1}{2\tau_\epsilon} \frac{s}{\tau} \left[-\Delta^{-1} \frac{1}{\tau_u} \frac{\partial^2 L}{\partial y^2} (D\phi_{ss}) D \tau (\text{Id} - W\sigma'(\phi_{ss}))^{-1} \right] \\ \Delta &:= \left(\frac{\alpha}{\tau_u} + \frac{1}{\tau_\epsilon} \right) \text{Id} + \frac{1}{\tau_u} \frac{\partial^2 L}{\partial y^2} (D\phi_{ss}) D \left(\frac{1}{\tau} (\text{Id} - W\sigma'(\phi_{ss})) \right)^{-1} \frac{1}{\tau} Q \end{aligned} \quad (130)$$

Using the separation of timescales $\tau \ll \tau_\epsilon \ll \tau_u$, this simplifies to

$$\mathbb{E} [\tilde{u}(t)\epsilon(t)^\top] \approx -\frac{s}{2\tau_u} \frac{\partial^2 L}{\partial y^2} (D\phi_{ss}) D (\text{Id} - W\sigma'(\phi_{ss}))^{-1} \quad (131)$$

Remembering that $\tilde{u} = u_{\text{hp}}$, we get the following plasticity dynamics using Eq. 122:

$$\tau_Q \frac{d}{dt} \mathbb{E} [Q(t)^\top] := \tau_Q \frac{d}{dt} \bar{Q}(t) = \frac{s^2}{2\tau_u} \frac{\partial^2 L}{\partial y^2} (D\phi_{ss}) D (\text{Id} - W\sigma'(\phi_{ss}))^{-1} - \gamma_Q \bar{Q}(t) \quad (132)$$

with $\bar{Q}(t)$ the first moment of $Q(t)$. For $\gamma > 0$, these dynamics are stable and lead to

$$\mathbb{E} [Q_{ss}^\top] = \frac{s^2}{2\tau_u \gamma_Q} \frac{\partial^2 L}{\partial y^2} (D\phi_{ss}) D (\text{Id} - W\sigma'(\phi_{ss}))^{-1} \quad (133)$$

thereby concluding the proof. \square

Isolating the postsynaptic noise ϵ with a multicompartment neuron model. The feedback learning rule of Eq. 122 and the corresponding Proposition S10 represent the feedback learning idea in its simplest form. However, for this learning rule, the feedback synapses need some mechanism to isolate the postsynaptic noise ϵ from the (noisy) neural activity. Meulemans et al. [29, 50] solve this by considering a multicompartment model of the neuron, inspired by recent dendritic compartment models of the cortical pyramidal neuron [14, 17, 40]. Here, a feedback (apical) compartment integrates the feedback input Qu , a basal compartment integrates the recurrent and feedforward input $W\sigma(\phi) + Ux$ and a central (somatic) compartment combines the two other compartments together and transmits the output firing rate $\sigma(\phi)$ to the other neurons. In this model, we can assume that a part of the noise ϵ enters through the feedback compartment, and change the feedback learning rule to

$$\tau_Q \dot{Q} = -(Qu + s\epsilon^{\text{fb}}) u_{\text{hp}}^\top - \gamma_Q Q, \quad (134)$$

where $(Qu + s\epsilon^{\text{fb}})$ is the feedback compartment activity, and hence locally available for the synaptic updates. As $\mathbb{E}[Quu_{\text{hp}}^\top] = Q\mathbb{E}[u_{\text{hp}}u_{\text{hp}}^\top] = Q\Sigma_u$ with Σ_u the positive definite auto-correlation matrix of u_{hp} , the result of Proposition S10 can be adapted to $\mathbb{E} [Q_{ss}^\top] \propto M \frac{\partial^2 L}{\partial y^2} (D\phi)_{ss} D (\text{Id} - W\sigma'(\phi_{ss}))^{-1}$, with $M = (\Sigma_u + \gamma \text{Id})^{-1}$ a positive definite matrix. This new fixed point of Q also satisfies the column space condition of Eq. 119.

Improving the parameter updates. When the column space condition is not perfectly satisfied, as is the case with this direct linear feedback controller when multiple data points are used, the empirical performance can be improved by changing the parameter updates towards

$$\Delta W = \sigma'(\phi_*) Qu_* \sigma(\phi_*)^\top, \quad \Delta U = \sigma'(\phi_*) Qu_* x^\top \quad (135)$$

This learning rule uses the local derivative of the nonlinearity σ as a heuristic to prevent saturated neurons from updating their weights, which is known to improve performance in feedforward networks [29, 50].

Alignment results. We empirically tested the controller with direct linear feedback and trained feedback weights Q on the MNIST digit recognition task. Figure S1 shows that the updates of Eq. 135 are approximately aligned to the gradients $-\nabla_{\theta}\mathcal{H}(\theta)$ on the least-control objective, indicating that the feedback weight learning for Q is successful and the controller with direct linear feedback approximates the optimal control.

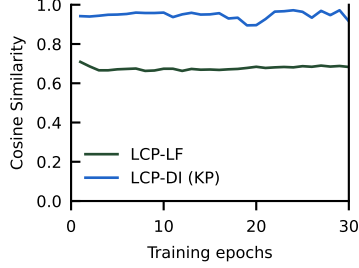


Figure S1: The linear feedback controller and inversion dynamics lead to approximate optimal control. Cosine similarity between the true gradient $-\nabla_W\mathcal{H}(\theta)$ and approximate updates ΔW of the least-control principle for training an equilibrium RNN on MNIST: a controller with trained linear feedback connections (LCP-LF) and a controller using dynamic inversion with trained feedback weights via Kolen-Pollack learning (LCP-DI KP).

S6.3.2 Simulation details

For computational efficiency, we run fixed-point iterations for finding the equilibrium of the controlled neural dynamics shown in Eq. 120, which in this case is equivalent to simulating the dynamics with the forward Euler method with a simulation stepsize equal to the timeconstant:

$$\begin{aligned}\phi_{\text{next}} &= W\sigma(\phi) + Ux + Qu \\ u_{\text{next}} &= (1 - \alpha)u - \frac{\partial L}{\partial y}(D\phi)\end{aligned}\quad (136)$$

We use the fixed points ϕ_* and u_* to update the parameters $\theta = \{W, U, b, \tilde{D}, \tilde{b}\}$ according to Eq. 116 with $\psi_* = Qu_*$. For training the feedback weights, we simulate the stochastic differential equations of Eq. 121 with the Euler-Maruyama method [98], starting from the fixed points computed in Eq. 136:

$$\begin{aligned}\epsilon_{\text{next}} &= \epsilon + \frac{\Delta t}{\tau_\epsilon} \left(-\epsilon + \frac{1}{\sqrt{\Delta t}} \Delta\xi \right) \\ \phi_{\text{next}} &= \phi + \frac{\Delta t}{\tau} (-\phi + W\sigma(\phi) + Ux + Qu + s\epsilon) \\ u_{\text{next}} &= u + \frac{\Delta t}{\tau_u} \left(-\frac{\partial L}{\partial y}(D\phi) - \alpha u \right)\end{aligned}\quad (137)$$

with Δt the simulation stepsize and $\Delta\xi \sim \mathcal{N}(0, \text{Id})$ white Gaussian noise that is drawn independently for each simulation step. The factor $\frac{1}{\sqrt{\Delta t}}$ in front of $\Delta\xi$ is due specific properties of Brownian motion in the simulation of stochastic differential equations. For computational efficiency, we accumulate the weight updates for Q over the simulation interval, and apply them at the end:

$$\Delta Q = -\frac{1}{\tau_Q} \left[\frac{1}{s^2} \sum_m (Qu[m] + \epsilon[m])(u[m] - u_*)^\top - \gamma Q \right]\quad (138)$$

where m is the simulation step and we use $u_{\text{hp}} = u - u_*$, with u_* the fixed point of Eq. (136), and where we scale by the noise variance s^2 to remove the dependence of the update magnitude on this hyperparameter. For all parameter updates, we use the Adam optimizer.

S6.3.3 Related work

This recurrent neural network model combined with the direct linear feedback controller Qu can be seen as a generalization of the Strong-DFC method [29] towards recurrent neural networks. Furthermore, the least-control principle provides a new theoretical foundation routed in optimal control. This enables us to derive the local update rules using constrained optimization theory, which

is more general and flexible compared to the theory based on the implicit function theorem used in Meulemans et al. [29]. For example, Meulemans et al. [29] use the assumption that Q is independent of θ and ϕ in their derivations, which is problematic when Q is trained to satisfy the column space condition of Theorem 2 which depends on θ and ϕ . In contrast, our Theorems 1 and 2 hold for general control mappings $Q(\phi, \theta)$ which can depend on θ and ϕ .

S6.4 Using general-purpose dynamics for computing an optimal control

In the main text (Section 3.1.2) we discussed the application of our two general-purpose optimal control methods to an equilibrium RNN. Here, we provide an expanded discussion on the neural network architectures each method yields. While we leave the development of more detailed biological models for future work, we comment on how these controlled RNNs may be implemented in cortical circuits, sketching a number of alternative circuit designs. We end this section by providing additional simulation and experimental details.

S6.4.1 Dendritic error compartments for dynamic inversion

In Section 3.1.2 we applied our general-purpose dynamic inversion method (8) to steer equilibrium RNNs towards optimally-controlled states. We restate here the resulting optimal control circuit (14) and discuss afterwards two possible network implementations, where feedback error signals are represented in dendritic compartments. Assuming without loss of generality that the output controller is of the leaky-integral kind, the resulting network dynamics (14) is:

$$\begin{aligned}\dot{\phi} &= -\phi + W\sigma(\phi) + Ux + \psi, \\ \dot{\psi} &= -\psi + \partial_{\phi}\sigma(\phi)S\psi + D^{\top}u, \\ \dot{u} &= -\alpha u - \nabla_y L(y).\end{aligned}\tag{139}$$

where $y = D\phi$ is the output neuron state, a subset of the full neuron state ϕ determined by a fixed selector matrix D . In what follows, we assume without further discussion that the output controller which integrates output errors $\nabla_y L(y)$ in time is implemented by means of some neural integrator circuit, a topic that has been extensively studied elsewhere [97].

In Eq. 139, the control variable ψ follows its own dynamics $\dot{\psi}$, which serves the purpose of inverting $\partial_{\phi}f(\phi, \theta)^{\top}$. This can be seen by inspecting the controlled steady state:

$$\psi_* = (\text{Id} - \partial_{\phi}\sigma(\phi_*)S)^{-1}D^{\top}u_*.\tag{140}$$

If the inverted factor appearing in the equation above would correspond to $\partial_{\phi}f(\phi_*, \theta)^{-\top}$, the network would be at an optimally-controlled state, where the weight updates following from our theory assume the Hebbian form

$$\begin{aligned}\Delta W &= \psi_*\sigma(\phi_*)^{\top}, \\ \Delta U &= \psi_*x^{\top}.\end{aligned}\tag{141}$$

For this to be the case, we need to satisfy the symmetry requirement $S = W^{\top}$. This corresponds to a form of weight transport, assuming that S and W are two distinct sets of synaptic connections.

We present now two alternative circuit implementations which allow maintaining $S \approx W^{\top}$ using local learning rules, so that the equations governing the change ΔW , ΔU and ΔS of all synaptic weights only depend on quantities presumed to be available pre- and post-synaptically and at the same time. In both cases, we build upon previous theories of error-driven cortical learning and assume that our control signal ψ corresponds to the apical dendritic activity of a cortical pyramidal cell, and ϕ to its somatic activity. According to this view, apical dendrites encode neuron-specific credit assignment signals ψ_* which are responsible for determining which neurons should potentiate or depress their connections, and by how much. We therefore extend previous models of apically-controlled synaptic plasticity [14, 18, 20, 23, 40], for which there is some experimental evidence [100], to the case of recurrently-connected networks.

Multiplexed codes. Interpreting our apical dendrite dynamics $\dot{\psi}$ in literal terms appears to require dendrodendritic synapses which bypass the soma, due to the apical-to-apical term $\psi \leftarrow S\psi$ occurring in (139). While such connections are known to exist in the brain [101], they are rare. We thus

highlight an alternative implementation, which builds on the interesting proposal that pyramidal cells might be capable of transmitting credit assignment signals alongside their intended outputs, by means of a multiplexed code [14, 23]. The basic premise of this theory is that certain synaptic connections are sensitive to high-frequency bursts of spikes only, which can be triggered by increasing apical activity, whereas other connections are tuned to filter out such events. Each connection type would then differentially reflect either apical or somatic activity, respectively; the required specific tuning to burst events or otherwise can be achieved for example by resorting to different profiles of short-term plasticity for each connection type. Here, we leverage on this idea and propose to replace the dendrodendritic (direct apical-to-apical) connections appearing in (139) by common (axodendritic) apical-targetting synapses mediated through the soma (i.e., soma-to-apical $\psi \leftarrow \phi$ synapses), tuned to be sensitive to burst events. This design enables keeping the circuit approximately symmetric ($S \approx W^\top$) through local burst-dependent plasticity rules, $\Delta S = \sigma(\phi_*)\psi_*^\top - \gamma S$ and $\Delta W = \psi_*\sigma(\phi_*)^\top - \gamma W$, a form of Kolen-Pollack learning [41, 53].

Interestingly, the resulting network model differs in a conceptually important – and experimentally testable – way from the multiplexing model originally proposed by Payeur et al. [23]: in our model, apical control signals should steer (thus, influence) the network state ϕ towards a controlled equilibrium, and therefore should *not* be filtered out from the somatic voltage dynamics $\dot{\phi}$, while the model of Payeur et al. [23] fully multiplexes credit assignment information and the actual computations carried out by the network. Critically, our major functional requirement is that apical-targetting connections be capable of selectively transmitting burst events (e.g., through short-term facilitating plasticity), and we make no further claims about the short-term plasticity of the remaining connections, leaving open the possibility of using this mechanism for other computational purposes unrelated to multiplexing.

Dendritic errors via lateral inhibition. Our network dynamics (139) is also compatible with an alternative proposal for how apical dendrites may come to encode credit assignment information, then used to steer synaptic plasticity within a neuron [17, 38]. In that model, dendritic errors emerge thanks to an auxiliary population of neurons, modeled after a particular class of inhibitory interneurons which preferentially target apical dendrites. These interneurons are set up such that they learn to reproduce the activity of pyramidal neurons. Both pyramidal neurons and interneurons feedback to apical dendrites, but with opposite sign. Sacramento et al. [17] showed that when the interneurons perfectly track pyramidal neurons (sometimes referred to as a ‘tight’ inhibitory-excitatory balance [102]) and an output error is generated, the remaining steady-state apical activity corresponds to a backpropagated error.

We briefly sketch here a proof-of-concept mapping of our dynamics (139) onto this model, while leaving more realistic implementations to future work. We first replicate our recurrently-connected neurons with a population of interneurons, whose state we denote by δ , and let both types of neurons feedback onto apical dendrites. Now, we follow the supplementary analysis of ref. [17] and assume that both populations have exactly the same connectivity and weights, a condition to ensure successful tracking and error propagation, which can be reached with the local weight updates for the interneurons introduced in ref. [17]. Moreover, for simplicity, here we assume our neurons are linear and ignore factors involving the derivative of the transfer function $\partial_\phi \sigma$, although it is possible to take such factors into account with a more detailed construction. Taking $\dot{\psi} = -\psi + S\phi - S\delta + D^\top u$ as our apical dendrite dynamics and inspecting its steady-state yields $\psi_* = (\text{Id} - S)^{-1}D^\top u_*$, as the interneuron activity perfectly tracks the pyramidal neuron activity $W\phi + Ux$, but does not include the apical activity ψ . This is the optimally-controlled equilibrium we sought. As with the multiplexed code described above, approximate symmetry $S \approx W^\top$ can then be maintained with local rules via Kolen-Pollack learning.

S6.4.2 Error neurons for energy-based dynamics

In the main text and in Sections S2.5 and S4, we have seen that the optimal control problem arising under our principle can be generically approached using a (constrained) energy-minimizing dynamics. We restate here the simple gradient-flow dynamics (15) presented in the main text:

$$\begin{aligned}\dot{\phi} &= -\psi + \partial_\phi \sigma(\phi) S \psi + D^\top u, \\ \psi &= \phi - W \sigma(\phi) - Ux,\end{aligned}\tag{142}$$

where u can be any output controller which enforces the constraint that the loss L is minimized with respect to the output neural activity y . We now briefly discuss how this system can be implemented

using a predictive coding architecture featuring two distinct subpopulations of neurons, generalizing the model of Whittington and Bogacz [35] to the RNN setting. In this architecture, ψ is interpreted as the activity of a population of prediction error neurons, while ϕ corresponds to the activity of prediction neurons. Error neurons ψ act as comparators, which measure deviations of the actual state of prediction neurons ϕ from the expected state $\mu := W\sigma(\phi) - Ux$; in this model, such deviations dynamically adjust the predictions ϕ towards an optimally-controlled steady-state in which the output loss is minimal (c.f. Section S4). The critical architectural difference to the models of Whittington and Bogacz [35] and Rao and Ballard [55] is that in our case the expected state μ does not necessarily stem from different network layers. A hierarchically-structured connectivity matrix W is a special case of our model; we allow for top-down, lateral and bottom-up contributions to the expected states μ .

S6.4.3 Training deep equilibrium models with the least-control principle.

We use deep equilibrium models that consist out of three main modules: (i) an encoder $g(x, \theta)$ that maps the input x to the implicit layer ϕ , (ii) an implicit layer defined by $f(\phi, \theta) = 0$ where $g(x, \theta)$ is incorporated inside $f(\phi, \theta)$, and (iii) a decoder $h(\phi, \theta)$ that maps the implicit layer towards the output y .

When $h(\phi, \theta)$ is independent of θ , we can use the inversion dynamics of Eq. 8 or the energy-based dynamics of Eq. 10 to compute an optimal control ψ^* and use the first-order parameter updates of Theorem 1. To harvest the full power of deep equilibrium models, it is beneficial to train the decoder $h(\phi, \theta)$ as well. However, this poses the problem that the loss $L(h(\phi, \theta))$ is now dependent on θ and hence Theorem 1 cannot be applied out-of-the-box. There are two general approaches to solve this challenge: (i) similar to the vanilla equilibrium RNNs, we can extend the state ϕ with an extra set of output neurons to absorb the θ -dependent decoder $h(\phi, \theta)$ inside of the implicit layer; and (ii) we can use the extended version of the least-control principle derived in Section S2.2 that can handle θ -dependent losses, to derive the parameter updates.

Augmenting the implicit layer. We can use an augmented state $\bar{\phi}$ that concatenates the system states ϕ with an extra set of output neurons $\tilde{\phi}$. Next we augment the implicit layer $f(\phi, \theta)$ towards

$$\bar{f}(\bar{\phi}, \theta) = \begin{bmatrix} f(\phi, \theta) \\ h(\phi, \theta) - \tilde{\phi} \end{bmatrix}. \quad (143)$$

Now, we can use a fixed linear decoder $D = [0 \text{ Id}]$ to select the output states $\tilde{\phi}$ for the loss $L(D\bar{\phi})$, which now is independent of θ .

Using the least-control principle for θ -dependent losses. In Section S2.2, we extend the least-control principle to θ -dependent losses, and among others derive a first-order update when the decoder $h(\phi, \theta)$ is θ -dependent, which we restate below.

$$\frac{d}{d\theta} \mathcal{H}(\theta) = -\psi_*^\top \frac{\partial f}{\partial \theta}(\phi_*, \theta) - u_*^\top \frac{\partial h}{\partial \theta}(\phi_*, \theta) \quad (144)$$

This first-order learning rule equals the gradient when the inversion dynamics (8) or energy-based dynamics (10) are used for computing the optimal control ψ^* , in the limit of $\alpha \rightarrow 0$. Due to its simplicity and direct applicability to the deep equilibrium models, without the need to augment the implicit layer, we use this update in our experiments.

S6.4.4 Simulation details

Equilibrium RNNs. We use the following fixed point iterations for finding the equilibrium of the inversion dynamics of Eq. 14:

$$\begin{aligned} \phi_{\text{next}} &= W\sigma(\phi) + Ux + \psi \\ \psi_{\text{next}} &= \frac{\partial \sigma}{\partial \phi}(\phi)S\phi + D^\top u \\ u_{\text{next}} &= (1 - \alpha)u - \frac{\partial L}{\partial y}(D\phi)^\top \end{aligned} \quad (145)$$

The fixpoint iterations terminates for a given input when either the relative change in the norm of the dynamic states $\Phi = \{\phi\}$ or $\Phi = \{\phi, \psi, u\}$ is less than some threshold ϵ , i.e. $\frac{\|\Phi_t - \Phi_{t+1}\|^2}{\|\Phi_t\|\|\Phi_{t+1}\|} \leq \epsilon$, or when some iteration budget `max_steps` is exhausted.

When we learn the feedback weights S with Kolen-Pollack learning (LCP-DI KP), we use the following weight updates for S and W :

$$\Delta W = \psi_* \sigma(\phi)^\top - \gamma W, \quad \Delta S = \sigma(\phi) \psi_*^\top - \gamma S \quad (146)$$

with γ the weight decay parameter. When we do not train the feedback weights S (LCP-DI), we fix them towards the transpose of the recurrent weights $S = W^\top$ and we use standard weight update for W without weight decay (12).

Deep equilibrium models. We generalize the above fixed point iterations to more complex recurrent architectures, by using the abstract inversion dynamics of Eq. 8.

$$\begin{aligned} \phi_{\text{next}} &= \phi + f(\phi, \theta) + \psi \\ \psi_{\text{next}} &= \psi + \frac{\partial f}{\partial \phi}(\phi, \theta)^\top \psi + \frac{\partial h}{\partial \phi}(\phi, \theta)^\top u \\ u_{\text{next}} &= (1 - \alpha)u - \frac{\partial L}{\partial y}(h(\phi, \theta))^\top \end{aligned} \quad (147)$$

We use the first-order updates discussed in Eq. 144 for training the DEQs.

S6.5 Additional experimental details

Here, we provide additional details on the experiments introduced in Section 3.1, including the architecture of the networks, the used hyperparameters, possible data preprocessing and the used optimization algorithms.

S6.5.1 Training equilibrium RNNs on the MNIST digit classification task

We evaluate the least-control principle combined with the various feedback circuits introduced in Section 3.1 on the MNIST digit classification task [51], and compare their performance to recurrent backpropagation (RBP).

Data preprocessing and augmentation. No data preprocessing or augmentation was employed in our experiment.

Architecture. We use 256 recurrent units in the RNN used for the results of table 1. We include a trained decoder \bar{D} inside the recurrent layer, as detailed in Section S6.1 and Eq. 108. For the results shown in Fig. 2, we run the equilibrium RNN on MNIST with [23, 32, 45, 64, 90, 128, 181, 256] recurrent units. We use the tanh nonlinearity for all recurrent units, and include bias terms according to Eq. 109.

Optimization. For the classification benchmark, we train the models for 30 epochs of the MNIST train set, with a minibatch size of 64 and with the Adam optimizer [103]. When we learn the feedback weights S with Kolen-Pollack learning, we apply the weight decay after every gradient update, i.e. we apply it outside of the optimizer.

For training the feedback weights Q of the linear feedback controller, we run the stochastic dynamics in Eq. 137 for `max_steps` timesteps, and we update Q following Eq. 138 by averaging ΔQ over the minibatch. For the simulation of the stochastic dynamics, we use $\Delta t = \tau'^2$, $\tau = \tau'^2$, $\tau_\epsilon = \tau'$ and $\tau_u = 1$ for some hyperparameter τ' . Table S1 contains details on the used and scanned hyperparameters.

For the overparametrization experiments, we use the same hyperparameters except for a learning rate of 0.001 for both RBP and LCP-DI, with a cosine annealing scheduler [104] annealing the learning rate down to 0.0001 over a total training time of 50 epochs.

For all experiments, we use gradient clipping whereby the norm of the gradient, computed over all gradients concatenated into a single vector, is normalized to some value (chosen to be 10) whenever above it. The gradient clipping was particularly crucial for training the RBP model.

Hyperparameter	RBF	LCP-DI	LCP-DI (KP)	LCP-LF
num_epochs	30	30	30	30
batch_size	64	64	64	64
α	-	{0, 0.01, 0.1, 1 }	1	1
lr	{ 10^{-4} , $3 \cdot 10^{-4}$, 10^{-3} }	{ 10^{-4} , $3 \cdot 10^{-4}$, 10^{-3} }	{ $3 \cdot 10^{-4}$, 10^{-3} }	{ $3 \cdot 10^{-4}$, 10^{-3} }
optimizer	ADAM	ADAM	ADAM	ADAM
max_steps	{50, 200 , 800}	{50, 200, 800 }	{200, 800 }	{200, 800 }
ϵ	{ 10^{-5} , 10^{-4} , 10^{-3} }	{ 10^{-5} , 10^{-4} , 10^{-3} }	10^{-4}	10^{-4}
s	-	-	-	{ 0.01 , 0.1}
τ'	-	-	-	{0.1, 0.2 }
τ_Q	-	-	-	{10, 100 , 1000}
γ_Q	-	-	-	{ 10^{-4} , 10^{-3} , 10^{-2} }
γ	-	-	{ 10^{-5} , 10^{-4} , 10^{-3} }	-
Gradient clipping	Yes	Yes	Yes	Yes

Table S1: Hyperparameter search space for the RNN MNIST experiment. A grid search with one seed for each configuration was done to find the best parameters, which are marked in bold. The search space for LCP-DI (KP) and LCP-LF were based on the results of the hyperparameter search for LCP-DI.

Hyperparameter	RBF	LCP-DI
num_epochs	75	75
batch_size	64	64
α	-	3
lr	0.03	0.05
optimizer	SGD	SGD
scheduler	cos	cos
max_steps	200	800
ϵ	10^{-4}	10^{-4}
Gradient clipping	Yes	Yes

Table S2: Hyperparameter used for the DEQ CIFAR10 experiment.

	Train set		Test set	
	NLL	Accuracy	NLL	Accuracy
DEQ-RBP	0.2403±0.0027	92.50±0.14	0.6172±0.0097	80.14±0.20
DEQ-LCP	0.3218±0.0062	89.55±0.17	0.5874±0.0077	80.26±0.17

Table S3: Classification accuracy (%) and negative log likelihood (NLL) on the CIFAR10 train and test set, of a DEQ model trained by recurrent backpropagation (RBP) and least control (LCP). The reported mean±std is computed over 3 seeds.

S6.5.2 Training deep equilibrium models on the CIFAR-10 classification benchmark

Here, we train a Deep Equilibrium model and evaluate its performance on the CIFAR-10 image classification benchmarks [59]. We compare the performance of the DEQ model trained via either RBP or LCP.

Data preprocessing and augmentation. We normalize all images channel-wise by subtracting the mean and dividing by the standard deviation, which are computed on the training dataset. We employed no data augmentation in our experiments.

Architecture. The model consists of 3 sub-modules that are invoked sequentially: an encoder, an implicit module, and a decoder. The encoder consists in a single convolutional layer with bias, followed by a Batchnorm layer [105]. The implicit module finds the fixed point of the following equation:

$$f(\phi, x, \theta) = -\phi + \text{norm}(\text{ReLU}(\phi + \text{norm}(x + c_2(\text{norm}(\text{ReLU}(c_1(\phi))))))) \quad (148)$$

where both c_1, c_2 are convolutional layers, and norm are group normalization layers [106]. Finally, the decoder module contains a batchnorm layer, followed by an average-pooling layer of kernel size 8-by-8, and a final linear classification layer. All convolutional layers use 48 channels, a filter size of 3-by-3, padding of 1, and are without biases unless specified otherwise.

Optimization. We train the model by finding the equilibrium of the controlled dynamics using the fixed point iterations of Eq. 147 and we update the parameters with the first order updates of Eq. 144. Both RBP and LCP-DI are trained on 75 epochs. We use the stochastic gradient descent optimizer with a minibatch size of 64, combined with an annealing learning rate using the cosine scheduler [104] which divides the learning rate by 10 over the training epochs. Table S2 contains further details on the hyper parameters.

Additional results. In table S3 we show additional experimental results for the CIFAR10 experiments. Note that the hyperparameter was chosen to maximise the test set accuracy. As can be seen, the training loss is not close to 0, indicating that the model considered here is not overparametrized enough for perfectly fitting the training set. Yet, LCP still manages to optimize for the training loss, and crucially, in such a way that generalizes competitively.

	Natural		Text	
	1L-256D	1L-512D	1L-256D	1L-512D
SIREN (input inj.)	22.88 ± 3.0	24.52 ± 3.28	24.54 ± 2.19	25.69 ± 2.18
iSIREN	24.28 ± 3.37	24.92 ± 3.58	26.06 ± 2.18	26.81 ± 2.09
INR-RBP	24.72 ± 3.90	25.47 ± 4.16	25.34 ± 1.67	26.53 ± 2.40
INR-LCP	24.25 ± 2.72	25.11 ± 2.90	26.71 ± 2.40	27.53 ± 2.00

Table S4: Peak signal-to-noise ratio (PSNR; in dB) for all models on the natural image and text generalization task [10]. The reported mean ± std is taken over the individual PSNR of the 16 images. SIREN and iSIREN results are taken from Huang et al. [10]. Note that while our INR model is trained without spectral normalization, we reach competitive results. Interestingly, LCP does perform on par with RBP while not relying on weight-decay, learning-rate scheduling or gradient clipping.

S6.5.3 Neural implicit representations

Inspired by the recent success of using implicit layers for implicit neural representations [10], we investigate using the least-control principle in this setup for learning. Implicit neural representations (INRs) are a quickly emerging field in computer vision and beyond with the aim to represent any signal through a continuous and differentiable neural network. Here we strictly follow the experimental setup of Huang et al. [10] and leverage the continuity of implicit neural representations to generalize on trained images. In particular, given an Image I , we train the INR to represent 25% of the pixels (we simply jump over every second pixel and every second row) while testing the networks prediction on 25% of unknown pixels and measuring the peak signal-to-noise ratio (PSNR). This can be regarded as simple image inpainting.

Architecture. Compared to Huang et al. [10], we slightly modify the implicit layer resulting in the following free dynamics

$$f_{\text{INR}}(\phi; x) = -\phi + \text{ReLU}(W\phi) + Ux. \quad (149)$$

We include a trained decoder matrix \tilde{D} inside the implicit layer, as discussed in Section S6.1. We use fixed point iterations on the inversion dynamics (147) for finding an optimal control, and use the weight updates for the equilibrium RNNs (116). Note that we did not include spectral normalization or a learning rate scheduler to train our models as in Huang et al. [10]. Despite these simplifications we obtain comparable results across methods and models.

Hyperparameters. Note the small discrepancy between the INR models trained with RBP and LCP-DI in Table S5. Interestingly, we had an easier time scanning hyperparameters to obtain competitive performance and stable forward dynamics when using LCP-DI compared to RBP, for which we had to include gradient clipping and weight decay. See Table S5 for the hyperparameters found when repeating the the grid search identical to the one seen in Table S1. Following Huang et al. [10], we include an extra hyperparameter (Ω), which is a scalar multiplier applied to all neural activity, and we scale the initialization of the weights accordingly with $1/\Omega$.

Additional results. Table S4 shows the full experimental results for learning neural implicit representations on the natural images and text dataset introduced by Huang et al. [10]. As we changed the network architecture slightly, we include the SIREN and iSIREN results of Huang et al. [10] for comparison. We see that the least-control principle achieves competitive performance on this task, compared to RBP and the results of Huang et al. [10].

Hyperparameter	RBF-Natural	LCP-Natural	RBF-Text	LCP-Text
iteration per image	500	500	500	500
α	-	0	-	0
lr	0.0001	0.0001	0.0001	0.0001
optimizer	Adam	Adam	Adam	Adam
max_steps	50	50	50	50
ϵ	10^{-5}	10^{-5}	10^{-5}	10^{-5}
weight decay	0.1	0.1	0.1	0.1
Omega	15	35	35	50
Gradient clipping	Yes	No	Yes	No

Table S5: Hyperparameter used for the INR experiments.

S7 The least-control principle for meta-learning

In Section 3.2, we consider a meta-learning problem in which the objective is to improve the performance of a learning algorithm as new tasks are encountered. To do so, we equip a neural network with fast weights ϕ that are learned on each task, and slow parameters $\theta = \{\omega, \lambda\}$ that parametrize the learning algorithm. The fast weights ϕ quickly learn how to solve a task τ and λ determines how strongly ϕ is pulled towards the slow weights ω , which consolidate the knowledge that has been previously acquired. The capabilities of the learning algorithm are then measured by evaluating $L_\tau^{\text{eval}}(\phi_\tau^*)$, the performance of the learned neural network on data from task τ that was held out during learning. Meta-learning finally corresponds to improving the learning performance on many tasks by adjusting the meta-parameters $\theta = \{\omega, \lambda\}$. This can be formalized through the following bilevel optimization problem [30, 67]:

$$\min_{\theta} \mathbb{E}_\tau [L_\tau^{\text{eval}}(\phi_\tau^*)] \quad \text{s.t.} \quad \phi_\tau^* = \arg \min_{\phi} L_\tau^{\text{learn}}(\phi) + \sum_i \frac{\lambda_i}{2} (\phi_i - \omega_i)^2. \quad (150)$$

Note that compared to Eq. 16 in the main text, we now consider the more general setting in which each synapse i has its own attraction strength λ_i and meta-learn them.

We now derive the update rules prescribed by the least-control principle, review the meta-learning algorithms we are comparing against and detail our experimental setup.

S7.1 Derivation of the meta-parameter updates

The first step of the derivation is to replace the $\arg \min$ in Eq. 150 by the associated stationarity condition:

$$\nabla_{\phi} L_\tau^{\text{learn}}(\phi_\tau^*) + \lambda(\phi_\tau^* - \omega) = 0. \quad (151)$$

This equation can be obtained from a dynamical perspective: let us assume that our learning algorithm is gradient descent, so that

$$\dot{\phi} = f(\phi, \theta) = -\nabla_{\phi} L_\tau^{\text{learn}}(\phi) - \lambda(\phi - \omega). \quad (152)$$

The stationarity conditions therefore correspond to $f(\phi_\tau^*, \theta) = 0$ and we can apply the least control principle.

To do so, we run the controlled dynamics

$$\dot{\phi} = -\nabla_{\phi} L_\tau^{\text{learn}}(\phi) - \lambda(\phi - \omega) + u, \quad \text{and} \quad \dot{u} = -\alpha u - \nabla_{\phi} L_\tau^{\text{eval}}(\phi), \quad (153)$$

and note ϕ_τ^* and u_τ^* the equilibrium. Note that this corresponds to taking $Q = \text{Id}$ and $h(\phi) = \phi$ in the general feedback dynamics of Eq. 6. Theorem 2 therefore guarantees that ϕ_τ^* is an optimally controlled state and u_τ^* an optimal control in the limit $\alpha \rightarrow 0$, as long as $\partial_{\phi} f(\phi_\tau^*, \theta)$ and $\partial_y^2 L(h(\phi_\tau^*))$ are invertible, and the column space condition

$$\text{col}[Q] = \text{row} \left[\frac{\partial h}{\partial \phi}(\phi_\tau^*) \frac{\partial f}{\partial \phi}(\phi_\tau^*, \theta)^{-1} \right] \quad (154)$$

is satisfied. The column space conditions here rewrites

$$\text{col}[\text{Id}] = \text{row} \left[\left(\frac{\partial^2 L_\tau^{\text{learn}}}{\partial \phi^2}(\phi_*^\tau) + \lambda \text{Id} \right)^{-1} \right], \quad (155)$$

and is automatically satisfied through the assumption that the Jacobian of f is invertible. To summarize, the controlled dynamics are optimal in the limit $\alpha \rightarrow 0$, if $\partial_y^2 L_\tau^{\text{learn}}(\phi_*^\tau) + \lambda \text{Id}$ and $\partial_y^2 L_\tau^{\text{eval}}(\phi_*^\tau)$ are invertible.

We now put ourselves in a regime in which the conditions detailed above are satisfied, so that $\phi_*^\tau = \phi_*^*$ and $u_*^\tau = u_*^*$. Theorem 1 then gives

$$\Delta \theta = - \left(\frac{d}{d\theta} \mathcal{H}(\theta) \right)^\top = \frac{\partial f}{\partial \theta}(\phi_*^\tau, \theta)^\top u_*^\tau = - \frac{\partial f}{\partial \theta}(\phi_*^\tau, \theta)^\top f(\phi_*^\tau, \theta), \quad (156)$$

as $\psi = Qu$ is here equal to u . A simple calculation gives

$$\begin{aligned} \frac{\partial f}{\partial \omega}(\phi_*^\tau, \theta) &= \text{diag}(\lambda) \\ \frac{\partial f}{\partial \lambda}(\phi_*^\tau, \theta) &= -\text{diag}(\phi_*^\tau - \omega), \end{aligned} \quad (157)$$

where $\text{diag}(x)$ is a diagonal matrix whose diagonal values are the elements of the vector x . It further implies that the updates of the parameters are local, as

$$\begin{aligned} \Delta \omega &= \lambda u_*^\tau = \lambda (\nabla_\phi L_\tau^{\text{learn}}(\phi_*^\tau) + \lambda(\phi_*^\tau - \omega)) \\ \Delta \lambda &= -(\phi_*^\tau - \omega) u_*^\tau = -(\phi_*^\tau - \omega) (\nabla_\phi L_\tau^{\text{learn}}(\phi_*^\tau) + \lambda(\phi_*^\tau - \omega)), \end{aligned} \quad (158)$$

the multiplications being performed element wise.

S7.2 Comparison to existing meta-learning algorithms

We here review existing meta-learning rules that we compare against in Section 3.2. We separate those methods in two categories, the one relying on implicit differentiation and the Reptile algorithm [75].

Implicit differentiation methods. The first set of methods we are reviewing aims at directly minimizing the bilevel optimization problem (150) using the implicit gradient

$$\frac{d}{d\theta} L_\tau^{\text{eval}}(\phi_*^\tau) = \frac{\partial L_\tau^{\text{eval}}}{\partial \phi}(\phi_*^\tau) \left(\frac{\partial^2 L_\tau^{\text{train}}}{\partial \phi^2}(\phi_*^\tau) + \text{diag}(\lambda) \right)^{-1} \frac{\partial^2}{\partial \theta \partial \phi} \left[\sum_i \frac{\lambda_i}{2} (\phi_{\tau,i}^* - \omega_i)^2 \right]. \quad (159)$$

In practice, this quantity is intractable because of the inverse of the Hessian and has to be estimated. This lead to different algorithms. T1-T2 [74] uses a first-order approximation of the implicit gradient by simply ignoring the inverse Hessian term:

$$\Delta \omega_i^{\text{T1-T2}} = \lambda_i \frac{\partial L_\tau^{\text{eval}}}{\partial \phi_i}(\phi_*^\tau), \quad \text{and} \quad \Delta \lambda_i^{\text{T1-T2}} = -(\phi_{\tau,i}^* - \omega_i) \frac{\partial L_\tau^{\text{eval}}}{\partial \phi_i}(\phi_*^\tau). \quad (160)$$

Alternatively, a better estimate of the gradient can be obtained by iteratively minimizing the quadratic form

$$\pi \mapsto \pi \frac{1}{2} \left(\frac{\partial^2 L_\tau^{\text{train}}}{\partial \phi^2}(\phi_*^\tau) + \text{diag}(\lambda) \right) \pi^\top + \pi \frac{\partial L_\tau^{\text{eval}}}{\partial \phi}(\phi_*^\tau) \quad (161)$$

and updating the meta-parameters with

$$\Delta \omega_i^{\text{Impl}} = -\lambda_i \pi_{\tau,i}^*, \quad \text{and} \quad \Delta \lambda_i^{\text{Impl}} = (\phi_{\tau,i}^* - \omega_i) \pi_{\tau,i}^*, \quad (162)$$

where π_τ^* is the result of the minimization procedure. Using gradient descent to minimize the quadratic form (161) yields the recurrent backpropagation algorithm [31, 32, 107, RBP], also known as Neumann series approximation in this context [76], we discussed in more details in Section S3. Gradient descent is a generic algorithm and more specialized optimization algorithms exist for quadratic forms, such as the conjugate gradients one used by Rajeswaran et al. [67, iMAML]. Note that the updates (158), (160) and (162) share some similar structure, but do not incorporate the

teaching signal in the same one. The update of T1-T2 does not correspond to any gradient, but the other two do. The estimation of the implicit gradient through Eq. 162 requires computing second derivatives, whereas the other two updates don't need to.

The implicit gradient can be approximated in a totally different way, using the equilibrium propagation theorem [24], as done by the contrastive meta-learning rule [30]. The idea is to first minimize the so-called augmented loss

$$\mathcal{L}_\tau(\phi, \theta, \beta) := L_\tau^{\text{learn}}(\phi) + \sum_i \frac{\lambda_i}{2} (\phi_i - \omega_i)^2 + \beta L_\tau^{\text{eval}}(\phi) \quad (163)$$

for two different values of β ($\beta = 0$ and some small positive value, note $\phi_{\tau,0}^*$ and $\phi_{\tau,\beta}^*$ the solutions) and then update the meta-parameters with

$$\Delta\omega_i^{\text{CML}} = \frac{\phi_{\tau,\beta,i}^* - \phi_{\tau,0,i}^*}{\beta}, \quad \text{and} \quad \Delta\lambda_i^{\text{CML}} = -\frac{(\phi_{\tau,\beta,i}^* - \omega_i)^2 - (\phi_{\tau,0,i}^* - \omega_i)^2}{2\beta}. \quad (164)$$

The equilibrium propagation theorem guarantees that those updates will converge to the true gradient when $\beta \rightarrow 0$. Both the contrastive meta-learning rule and the rule prescribed by our principle are first-order, as that they don't require computing second derivative. However, the former approximates the implicit gradient when the latter approximates the gradient of the least-control objective \mathcal{H} . Interestingly, as we mentioned in Section 2.4, the augmented solution ϕ_β^* and the controlled equilibrium ϕ_τ^* are both stationary points of the augmented loss \mathcal{L}_τ (taking $\beta = \alpha^{-1}$ for ϕ_τ^*). However, the contrastive meta-learning update (164) is justified in the weak nudging limit ($\beta \rightarrow 0$), whereas the update (158) is justified in the perfect control limit ($\alpha = \beta^{-1} \rightarrow 0$).

We refer to Zucchet and Sacramento [108] for a more detailed review of those methods.

Reptile. The Reptile algorithm [75] meta-learns the initialization of a neural network such that it can adapt to a new task τ in very few gradient descent steps. Let us denote ω the parameters of the network at initialization. The Reptile algorithm first minimizes the learning loss $L_\tau^{\text{learn}}(\phi)$ and then update ω through

$$\Delta\omega^{\text{Reptile}} = \phi_\tau^* - \omega, \quad (165)$$

with ϕ_τ^* the result of the learning loss minimization. Contrary to the methods presented above, this algorithm is only heuristically motivated and does not rely on any theoretical foundations. Still, it performs surprisingly well on many few-shot learning tasks.

S7.3 Experimental details

We compare the LCP to existing meta-learning and few-shot learning algorithms on the Omniglot few-shot image classification benchmark [77]. We follow the standard training and evaluation used in prior works [67, 73]. We focus on the 20-way 1-shot setting, and only meta-learn $\theta = \{\omega\}$ while choosing a global λ as a hyperparameter. The iMAML result in Table 3.2 is taken from Rajeswaran et al. [67] while those of Reptile and FOMAML are taken from Nichol et al. [75].

Data preprocessing and augmentation. We resize the Omniglot images to 28×28 and augment the images by random rotation by multiples of 90 degrees during meta-training.

Architecture. For our classifier, we use the same architecture as in previous works [67, 73], which consists in 4 convolutional modules with a 3×3 convolutions and 64 filters, each followed by a batch normalization layer, a ReLU nonlinearity, and a 2×2 max-pooling layer. The output of the module is then flattened and fed into a final classification layer followed by a softmax activation.

Optimization. We train all models on 100000 tasks, split into meta batches of size 16. Each task consists in a 20-way classification problem with a single example per class provided for the adaptation phase, and 15 examples per class for evaluating the adaptation. For T1-T2, the adaptation consists in 100 gradient steps with learning rate $\eta = 0.03$. For LCP, we use 100 steps of the discretized version of the dynamics (153):

$$\begin{aligned} \phi_{\text{next}} &= \phi + \eta \left(-\nabla_\phi L_\tau^{\text{learn}}(\phi) - \lambda(\phi - \omega) + u \right) \\ u_{\text{next}} &= u + \eta \left(-\alpha u - \nabla_\phi L_\tau^{\text{eval}}(\phi) \right), \end{aligned} \quad (166)$$

Hyperparameter	T1-T2	LCP
num_tasks	100000	100000
meta_batch_size	16	16
optimizer_outer	ADAM	ADAM
lr_outer	0.001	0.001
steps_inner	100	100
η	0.03	0.03
α	-	0.1
λ	0.001	0.001

Table S6: Hyperparameter used for the 20-way 1-shot Omniglot experiment.

where $\eta = 0.03$. The Adam optimizer takes the $\Delta\omega$ as input and updates the meta-parameters, with learning rate 0.001. Finally, the models are evaluated on 100 test tasks. See Table S6 for an overview of the hyperparameters.